Accepted Manuscript

Design and synthesis of new ruthenium polypyridyl complexes with potent antitumor activity in vitro

Guang-Bin Jiang, Wen-Yao Zhang, Miao He, Yi-Ying Gu, Lan Bai, Yang-Jie Wang, Qiao-Yan Yi, Fan Du

PII:	S1386-1425(19)30513-X
DOI:	https://doi.org/10.1016/j.saa.2019.05.037
Reference:	SAA 17132
To appear in:	*Spectrochimica Acta Part A: Molecular and Biomolecular Spectroscopy*
Received date:	17 March 2019
Revised date:	6 May 2019
Accepted date:	12 May 2019

Please cite this article as: G.-B. Jiang, W.-Y. Zhang, M. He, et al., Design and synthesis of new ruthenium polypyridyl complexes with potent antitumor activity in vitro, Spectrochimica Acta Part A: Molecular and Biomolecular Spectroscopy, https://doi.org/10.1016/j.saa.2019.05.037

Submitted to Spectrochimica Acta Part A: Molecular and Biomolecular Spectroscopy

Design and Synthesis of New Ruthenium Polypyridyl Complexes with Potent Antitumor Activity in Vitro

Guang-Bin Jiang,[a,*] Wen-Yao Zhang,[b] Miao He,[b] Yi-Ying Gu,[b] Lan Bai,[b] Yang-Jie Wang,[b] Qiao-Yan Yi,[b] Fan Du[b]

[a]*Guangxi Key Laboratory of Electrochemical and Magneto-chemical Function Materia, College of Chemistry and Bioengineering, Guilin University of Technology, Guilin, 541004, China.*

[b]*School of Pharmacy, Guangdong Pharmaceutical University, Guangzhou, 510006, PR China*

* Corresponding authors. Tel: +86-773-899-1304; fax: +86-773-899-1304.

E-mail address: jianggb@glut.edu.cn (G.B. Jiang).

Abstract We herein report the synthesis, characterization and anticancer activity of BTPIP (2-(4-(benzo[*b*]thiophen-2-yl)phenyl)-1*H*-imidazo[4,5-*f*][1,10]phenanthroline) and its four ruthenium(II) polypyridyl complexes $[Ru(N\text{-}N)_2(BTPIP)](ClO_4)_2$ (N-N = bpy = 2,2′-bipyridine, **Ru(II)-1**; phen = 1,10-phenanthroline, **Ru(II)-2**; dmb = 4,4′-dimethyl-2,2′-bipyridine, **Ru(II)-3**; dmp = 2,9-dimethyl-1,10-phenanthroline, **Ru(II)-4**). The DNA binding behaviors reveal that the complexes bind to calf thymus DNA by intercalation. Cytotoxicity of the complexes against A549, HepG-2, SGC-7901 and Hela cells were evaluated in vitro. Complexes **Ru(II)-1**, **Ru(II)-2**, **Ru(II)-3, Ru(II)-4** show moderate activity on the cell proliferation in A549 cells with IC_{50} values of 9.3 ± 1.2, 12.1 ± 1.6, 10.3 ± 1.6, 8.9 ± 1.2 μM, respectively. Apoptosis assessment, intracellular mitochondrial membrane potential (MMP), location in mitochondria, reactive oxygen species (ROS), cell invasion assay and cell cycle arrest were also performed to explore the mechanism of this action. When the concentration of the ruthenium(II) complexes is increased, the amount of reactive oxygen species increases obviously and the mitochondrial membrane potential decreases dramatically in A549 cells. Most importantly, the ruthenium(II) polypyridyl complexes could arrive the cytoplasm through the cell membrane and accumulate in the mitochondria. These results showed that the ruthenium(II) complexes could induce apoptosis in A549 cells through an ROS-mediated mitochondrial dysfunction pathway.

Keywords: Ruthenium(II) complex; antitumor; intercalation; reactive oxygen species; mitochondrial membrane potential.

1. Introduction

Platinum-based anticancer drugs, including cisplatin, carboplatin and oxaliplatin, have been widely used in the field of antitumor chemotherapies and continue to represent the mainstay of therapy for various cancer types [1-8]. However, platinum-based anticancer drugs also show many shortcomings, such as nephrotoxicity, myelotoxicity, neural damage, ototoxicity, and strong resistance, which prompted to search the alternative metal-based anticancer drugs with high efficient and selectivity [9-13].

It was believed that the complexes containing ruthenium display low toxicity, easily absorbed and rapidly excreted by the body, and will become one of the most promising antitumor drugs [14-19]. Therefore, during the past decades, remarkable efforts have been devoted to synthesis ruthenium-based anticancer drugs [20-28]. For instance, Wong and co-workers demonstrated that $[Ru(N\text{-}N)_2\text{-}(p\text{-MOPIP})](PF_6)_2\cdot 2H_2O$ (N-N = 2,2′-bipyridine (bpy); 1,10-phenanthroline (phen); 4,4′-dimethyl-2,2′-bipyridine (dmb); PIP = 2-phenylimidazo[4,5-*f*][1,10]phenanthroline) can induce mitochondria-mediated and caspase-dependent apoptosis in various cancer cells [29]. The Maysinger group reported that ruthenium(II)-letrozole complexes can effectively inhibit the proliferation of MCF-7 and U251N cells [30]. In 2015, Chao found that four ruthenium(II) complexes can utilize as mitochondria-targeted two-photon photodynamic anticancer agents [31]. Very recently, the group of Liu described that $[Ru(phen)_2(PFPIP)](ClO_4)_2]$, a Ru(II) complex with high antitumor activity, was able

to effectively inhibit growth of HepG-2 cells [32].

It is well known that heterocyclic compounds have been reported to possess remarkable anticancer, anti-inflammatory, antibacterial, antioxidant, antidiabetic, immuomodulatory, and anti-HIV activities [23-35]. Among them, thiophene-containing compounds have been attracted more attention owing to their wide range of biological properties [36-38]. Nonetheless, thiophene-containing ruthenium complexes are rarely investigated as anticancer drugs. In continuation of our interest in the field of antitumor, herein, a thiophene-containing ligand BTPIP and its four ruthenium(II) polypyridyl complexes $[Ru(bpy)_2(BTPIP)](ClO_4)_2$ (**Ru(II)-1**), $[Ru(phen)_2(BTPIP)](ClO_4)_2$ (**Ru(II)-2**), $[Ru(dmb)_2(BTPIP)](ClO_4)_2$ (**Ru(II)-3**), and $[Ru(dmp)_2(ETPIP)](ClO_4)_2$ (**Ru(II)-4**) (Scheme 1) were synthesized and characterized by ^1H NMR, ^{13}C NMR, HRMS and IR. The interaction of the Ru(II) polypyridyl complexes with CT DNA was investigated via electronic absorption titration, viscosity measurements and luminescence spectra. In addition, the anticancer activities of these complexes were firstly examined in vitro against the A549, HepG-2, SGC-7901 and Hela cancer cell lines. Most importantly, the possible antitumor mechanism of the Ru(II) complexes were detected by determining the cells morphological changes, cell cycle arrest, ROS levels and the decrease of the mitochondrial membrane potentials.

2. Experimental section

2.1. Materials and methods

All reagents and solvents were purchased commercially and used without further purification unless otherwise noted. Calf thymus DNA (CT DNA) was obtained from the Sino American Biotechnology Company. Ltd. Ultrapure MilliQ water was used in all experiments. DMSO and RPMI 1640 were purchased from Sigma. Cell lines of HeLa (Human cervical cancer cell line), SGC-7901 (human gastric carcinoma cells), HepG-2 (Hepatocellular carcinoma cells) and A549 (Human lung carcinoma cells) were purchased from the American Type Culture Collection. $RuCl_3 \cdot 3H_2O$ was obtained from the Kunming Institution of Precious Metals. 2,2′-Bipyridine, 1,10-phenanthroline, 4,4′-dimethyl-2,2′-bipyridine, 2,9-dimethyl-1,10-phenanthroline were obtained from the Guangzhou Chemical Reagent Factory.

Analytical thin layer chromatography was performed by using commercially prepared 100-400 mesh silica gel plates (GF_{254}) and visualization was effected at 254 nm. Mass spectra were recorded on a Thermo Scientific ISQ gas chromatograph-mass spectrometer. The data of HRMS was carried out on a high-resolution mass spectrometer (LCMS-IT-TOF). IR spectra were obtained either as potassium bromide pellets or as liquid films between two potassium bromide pellets with a Bruker TENSOR 27 spectrometer. ^{1}H NMR spectra were recorded on a Varian-500 spectrometer with DMSO-d_6 as solvent and tetramethylsilane (TMS) as an internal standard at 400 MHz at room temperature.

2.2. Synthesis of ligand and complexes

2.2.1. Synthesis of 4-(benzo[b]thiophen-2-yl)benzaldehyde

To a resealable Schlenk tube or alternatively, a screw-cap pressure tube, were added 4-bromobenzaldehyde (1.0 mmol, 1.0 equiv), $Pd(OAc)_2$ (5 mol %), benzo[*b*]thiophen-2-ylboronic acid (1.5 mmol, 1.5 equiv), K_2CO_3 (2 mmol, 2 equiv), toluene (6 mL) and a stir bar. The reaction vessel was fitted with a rubber septum, and was evacuated and back-filled with nitrogen. The reaction tube was sealed and immersed in a preheated oil bath at 100 °C for 12 h and the solution was stirred with the aid of a magnetic stirrer. After attaining ambient temperature, the reaction mixture was diluted with ethyl acetate and filtered through a plug of silica gel. The filtrate was concentrated and the resulting residue was purified by column chromatography (silica gel, petroleum ether/EtOAc) to give the desired aldehydes.

2.2.2. Synthesis of ligand (BTPIP)

A mixture of 1,10-phenanthroline-5,6-dione (100.0 mg, 0.5 mmol), 4-(benzo[*b*]thiophen-2-yl)benzaldehyde (119.0 mg, 0.5 mmol), ammonium acetate (15 mmol, 1156.2 mg) and acetic acid (30 mL) was refluxed with stirring for 4 h. The cooled solution was diluted with water and neutralized with concentrated aqueous ammonia. The brown precipitate was collected and purified by column chromatography on silica gel (60~100 mesh) with ethanol as eluent to give the compound as a brown yellow powder. Yield: 188.3 mg, 88%. Anal. Calc for $C_{27}H_{16}N_4S$: C, 75.68; H, 3.76; N, 13.07%. Found: C, 75.80; H, 3.71; N, 12.99%; IR: ν = 3101, 2102, 1916, 1793, 1691, 1597, 1588, 1480, 1358, 1312, 1188, 1121, 953, 819, 736, 682 cm^{-1}; ^1H NMR (400 MHz, DMSO-d_6) δ 9.03 (d, J = 4.0 Hz, 2H, a, a′), 8.94

(d, *J* = 8.1 Hz, 2H, c, c′), 8.40 (dd, *J* = 22.3, 8.3 Hz, 2H, j, k), 7.99 (d, *J* = 10.1 Hz, 5H, d, e,f, g, l), 7.88-7.80 (m, 3H, h, b, b′), 7.40 (t, *J* = 6.8 Hz, 1H, i); ^{13}C NMR (100 MHz, DMSO-d_6) δ 192.8 (1C, n′), 172.5 (1C, p), 150.4 (1C, a), 148.1 (1C, a′), 143.7 (1C, u), 142.9 (1C, t), 142.1 (1C, r), 140.9 (1C, n), 139.2 (1C, x), 134.8 (1C, v), 130.8 (1C, c), 130.4 (1C, c′), 130.2 (2C, d, g), 127.4 (1C, e, f), 127.0 (1C, s), 126.9 (1C, s′), 125.9 (1C, j), 125.5 (1C, k), 125.4 (1C, o), 124.7 (1C, i), 124.4 (1C, l), 123.8 (1C, o′), 123.0 (1C, b), 122.9 (1C, b′), 121.2 (1C, h); HRMS (ESI) m/z: calcd for $C_{27}H_{17}N_4S$ $[M+H]^+$, 429.1168; found 429.1169.

*2.2.3. Synthesis of [Ru(bpy)$_2$(BTPIP)](ClO$_4$)$_2$ (**Ru(II)-1**)*

A mixture of *cis*-[Ru(bpy)$_2$Cl$_2$]·2H$_2$O (158.7 mg, 0.3 mmol) and BTPIP (128.4 mg, 0.3 mmol) in ethylene glycol (12 mL) was heated at 150 ^{o}C under argon for 8 h to give a clear red solution. Upon cooling, a red precipitate was obtained by dropwise addition of saturated aqueous NaClO$_4$ solution. The crude product was purified by column chromatography on neutral alumina with a mixture of CH$_3$CN-toluene (1:1, v/v) as eluent. The red band was collected. The solvent was removed under reduced pressure and a red powder was obtained. Yield: 259.2 mg, 83%. Anal. Calc for $C_{47}H_{32}Cl_2N_8O_8RuS$: C, 54.24; H, 3.10; N, 10.77%. Found: C, 54.33; H, 3.02; N, 10.86%; UV-vis (5 μM; λ_{max}, 467 nm); IR: ν = 3073, 1603, 1511, 1479, 1463, 1446, 1313, 1272, 953, 827, 808, 765, 726, 624 cm^{-1}; ^{1}H NMR (400 MHz, DMSO-d_6) δ 9.05 (d, *J* = 8.1 Hz, 2H, a, a′), 8.81 (d, *J* = 8.2 Hz, 4H, 4, 4′, 5, 5′), 8.43 (s, 4H, 1, 1′, 8, 8′), 8.36 (d, *J* = 7.9 Hz, 2H, c, c′), 8.19 (d, *J* = 5.0 Hz, 2H, d, g), 8.13 (d, *J* = 4.9 Hz,

2H, e, f), 8.04-7.89 (m, 7H, h, l, i, b, b′, 3, 3′), 7.83-7.77 (m, 6H, k, j, 2, 2′, 6, 6′), 7.40 (dd, *J* = 14.7, 7.3 Hz, 2H, 7, 7′); ^{13}C NMR (100 MHz, DMSO-d_6) δ 158.8 (2C, n, n′), 158.5 (2C, 9, 9′), 153.3 (2C, 10, 10′), 153.2 (1C, p), 153.2 (2C, 1, 1′), 150.6 (2C, 8, 8′), 147.8 (2C, a, a′), 147.7 (1C, u), 145.9 (1C, t), 142.8 (1C, r), 140.9 (2C, 3, 3′), 139.3 (2C, 6, 6′), 137.3 (1C, x), 135.3 (1C, v), 130.9 (2C, c, c′), 131.0 (2C, d, g), 130.9 (1C, e), 128.9 (1C, f), 127.9 (2C, s, s′), 127.6 (2C, 4, 4′), 127.1 (2C, 5, 5′), 126.9 (1C, j), 126.8 (1C, k), 126.6 (2C, o, o′), 126.4 (1C, i), 125.5 (1C, l), 125.5 (2C, b, b′), 124.5 (2C, 2, 2′), 123.0 (2C, 7, 7′), 121.5 (1C, h); HRMS (ESI) m/z: calcd for $C_{47}H_{31}N_8SRu$ $[M\text{-}2ClO_4\text{-}H]^+$, 841.1442; found 841.1450.

*2.2.4. Synthesis of [Ru(phen)$_2$(BTPIP)](ClO$_4$)$_2$ (**Ru(II)-2**)*

This complex was synthesized in an identical manner to that described for complex **Ru(II)-1**, with *cis*-$[Ru(phen)_2Cl_2]\cdot 2H_2O$ [32,39] in place of *cis*-$[Ru(bpy)_2Cl_2]\cdot 2H_2O$. Yield: 254.8 mg, 78%. Anal. Calc for $C_{51}H_{32}Cl_2N_8O_8RuS$: C, 56.26; H, 2.96; N, 10.29%. Found: C, 56.41; H, 3.04; N, 10.21%; UV-vis (5 μM; λ_{max}, 465 nm); IR: *v* = 3051, 1601, 1576, 1508, 1478, 1455, 1426, 1363, 1304, 1250, 1224, 944, 843, 808, 750, 623, 528 cm^{-1}; ^{1}H NMR (400 MHz, DMSO) δ 9.13 (dd, J = 24.7, 7.9 Hz, 2H, a, a′), 8.90 (dd, J = 14.6, 8.1 Hz, 4H, 1, 1′, 8, 8′), 8.47 (dd, J = 41.7, 7.2 Hz, 2H, 3, 3′), 8.24 (t, J = 7.8 Hz, 2H, 6, 6′), 8.13 (t, J = 7.7 Hz, 2H, c, c′), 8.00 (t, J = 9.7 Hz, 4H, d, e, f, g), 7.96-7.81 (m, 7H, h, l, i, b, b′, 4, 4′), 7.70-7.61 (m, 4H, 5, 5′, 7, 7′), 7.41 (d, J = 6.3 Hz, 4H, k, j, 2, 2′); ^{13}C NMR (100 MHz, DMSO-d_6) δ 157.3 (2C, n, n′), 157.1 (2C, 9, 9′), 151.9 (2C, 10, 10′), 149.1 (1C, p), 149.2 (2C, a, a′), 149.3 (2C,

8, 8′), 145.2 (2C, a, a′), 145.1 (1C, u), 143.1 (1C, t), 141.0 (1C, r), 139.2 (1C, n), 138.4 (2C, 3, 3′), 138.2 (2C, 6, 6′), 134.5 (1C, x), 130.9 (1C, v), 128.4 (2C, c, c′), 128.2 (2C, d, g), 127.6 (2C, e, f), 127.7 (2C, 4, 4′), 126.8 (2C, 5, 5′), 126.2 (2C, s, s′), 126.3 (2C, 11, 11′), 125.4 (2C, 12, 12′), 125.5 (1C, j), 124.9 (1C, k), 125.0 (2C, o, o′), 124.8 (1C, i), 124.4 (1C, l), 123.0 (2C, 2, 2′), 121.0 (2C, 7, 7′), 115.4 (1C, h); HRMS (ESI) m/z: calcd for $C_{51}H_{31}N_8SRu$ $[M\text{-}2ClO_4\text{-}H]^+$, 889.1443; found 889.1451.

*2.2.5. Synthesis of $[Ru(dmb)_2(BTPIP)](ClO_4)_2$ (**Ru(II)-3**)*

This complex was synthesized in an identical manner to that described for complex **Ru(II)-1**, with *cis*-$[Ru(dmb)_2Cl_2]\cdot 2H_2O$ [32,39] in place of *cis*-$[Ru(bpy)_2Cl_2]\cdot 2H_2O$. Yield: 266.6 mg, 81%. Anal. Calc for $C_{51}H_{40}Cl_2N_8O_8RuS$: C, 55.84; H, 3.68; N, 10.21%. Found: C, 55.73; H, 3.57; N, 10.28%; UV-vis (5 μM; λ_{max}, 476 nm); IR: ν = 3057, 2919, 1618, 1507, 1479, 1448, 1364, 1304, 1197, 1093, 953, 825, 725, 566, 544 cm^{-1}; ^1H NMR (400 MHz, DMSO) δ 9.06 (dd, J = 13.5, 8.2 Hz, 2H, a, a′), 8.75 (d, J = 15.5 Hz, 4H, 3, 3′, 4, 4′), 8.39 (dd, J = 22.9, 7.7 Hz, 2H, 1, 1′), 7.98 (m, J = 31.6, 22.2, 5.8 Hz, 9H, 6, 6′, c, c′, d, e, f, g, h), 7.70 (s, 2H, l, i), 7.48-7.36 (m, 6H, b, b′, k, j, 2, 2′), 7.20 (s, 2H, 5, 5′), 2.58 (s, 6H, 7), 2.48 (s, 6H, 8); ^{13}C NMR (100 MHz, DMSO-d_6) δ 156.8 (2C, n, n′), 156.7 (2C, 9, 9′), 153.6 (2C, 10, 10′), 151.0 (1C, p), 150.9 (2C, 1, 1′), 150.0 (2C, 6, 6′), 149.9 (2C, a, a′), 149.8 (1C, u), 145.6 (1C, t), 142.9 (1C, r), 140.9 (1C, n), 139.3 (2C, 11, 11′), 135.1 (2C, 12, 12′), 135.0 (1C, x), 130.7 (1C, v), 130.5 (2C, c, c′), 129.4 (2C, d, g), 129.0 (2C, e, f), 128.8 (2C, s, s′), 127.7 (2C, 3, 3′), 127.0 (2C, 4, 4′), 127.0 (1C, j), 126.5 (1C, k), 125.5 (2C,

o, o′), 125.4 (1C, i), 124.4 (1C, l), 123.0 (2C, b, b′), 121.3 (2C, 2, 2′), 121.0 (2C, 5, 5′), 21.2 (2C, 7, 7′), 21.1 (2C, 8, 8′); HRMS (ESI) m/z: calcd for $C_{51}H_{39}N_8SRu$ $[M\text{-}2ClO_4\text{-}H]^+$, 897.2069; found 897.2077.

*2.2.6. Synthesis of $[Ru(dmp)_2(BTPIP)](ClO_4)_2$ (**Ru(II)-4**)*

This complex was synthesized in an identical manner to that described for complex **Ru(II)-1**, with *cis*-$[Ru(dmp)_2Cl_2]\cdot 2H_2O$ [32,39] in place of *cis*-$[Ru(bpy)_2Cl_2]\cdot 2H_2O$. Yield: 237.1 mg, 69%. Anal. Calc for $C_{55}H_{40}Cl_2N_8O_8RuS$: C, 57.69; H, 3.52; N, 9.79%. Found: C, 57.56; H, 3.61; N, 9.72%; UV-vis (5 μM; λ_{max}, 479 nm); IR: ν = 3053, 1964, 1605, 1588, 1507, 1478, 1433, 1348, 1248, 1216, 1089, 854, 809, 726, 622, 555 cm^{-1}; ^1H NMR (400 MHz, DMSO) δ 8.93 (d, J = 8.3 Hz, 2H, a, a′), 8.83 (d, J = 8.0 Hz, 2H, c, c′), 8.48-8.43 (m, 3H, 3, 3′, l), 8.28 (t, J = 10.2 Hz, 3H, 2, 2′, i), 8.02-7.96 (m, 4H, 6, 6′, 4, 4′), 7.94-7.87 (m, 3H, h, b, b′), 7.52-7.44 (m, 2H, d, g), 7.43-7.34 (m, 6H, e, f, 5, 5′, k, j), 7.19 (m, J = 34.5, 7.6 Hz, 2H, 1, 1′), 1.97 (s, 6H), 1.76 (s, 6H); ^{13}C NMR (100 MHz, DMSO-d_6) δ 168.4 (2C, n, n′), 166.8 (2C, 9, 9′), 150.7 (2C, 10, 10′), 150.3 (1C, p), 149.4 (2C, 13, 13′), 149.0 (2C, 14, 14′), 148.3 (2C, a, a′), 145.9 (1C, u), 143.6 (1C, t), 142.9 (1C, r), 140.9 (2C, 2, 2′), 139.2 (2C, 5, 5′), 138.6 (1C, x), 137.8 (1C, v), 137.2 (2C, c, c′), 135.0 (2C, d, g), 131.0 (2C, e, f′), 130.8 (2C, 11, 11′), 120.0 (2C, 12, 12′), 129.4 (1C, j), 128.7 (21C, k), 128.0 (1C, o), 127.9 (1C, i), 127.6 (1C, l), 127.0 (1C, b), 126.3 (1C,b′), 125.8 (1C, 1), 125.4 (1C, 1′), 124.4 (1C, 6), 123.0 (1C, 6′), 121.3 (1C, h), 26.0 (2C, 7, 7′), 25.0 (2C, 8, 8′); HRMS (ESI) m/z: calcd for $C_{55}H_{39}N_8SRu$ $[M\text{-}2ClO_4\text{-}H]^+$, 945.2070; found 945.2088.

Caution: Perchlorate salts of metal compounds with organic ligands are potentially explosive, and only small amounts of the material should be prepared and handled with great care.

2.3. Ruthenium(II) complexes-CT-DNA binding

The DNA-binding experiments were performed at room temperature. Buffer A [5 mM Tris-HCl, 50 mM NaCl, pH 7.0] was used for absorption titration, and viscosity measurements. Buffer B (50 mM Tris-HCl, 18 mM NaCl, pH 7.2) was used for DNA photocleavage experiments. Solutions of CT DNA in buffer A gave a ratio of UV-Vis absorbance of 1.8~1.9:1 at 260 and 280 nm, indicating that the DNA was sufficiently free of protein [40]. The concentration of DNA was determined spectrophotometrically (ε_{260} = 6600 M^{-1} cm^{-3}) [41].

The absorption titrations of the complex in buffer were performed using a fixed concentration (5.0 μM) for complex to which increments of the DNA stock solution were added. The intrinsic binding constant *K*, based on the absorption titration, was measured by monitoring the changes in absorption at the MLCT (metal-to-ligand charge transfer) band with increasing concentration of DNA using the following equation [42].

$$[DNA]/(\varepsilon_a - \varepsilon_f) = [DNA]/(\varepsilon_b - \varepsilon_f) + 1/[K_b((\varepsilon_b - \varepsilon_f)] \quad (1)$$

Where [DNA] is the concentration of DNA in base pairs, ε_a, ε_f and ε_b correspond to the apparent absorption coefficient A_{obsd}/[Ru], the extinction coefficient for the free ruthenium complex and the extinction coefficient for the ruthenium

complex in the fully bound form, respectively. In plots of [DNA]/(ε_a-ε_f) versus [DNA], K_b is given by the ratio of slope to the intercept.

The emission spectra of the complexes in buffer were performed using a fixed concentration (5 μM) for complexes to which increments of the CT DNA stock solution were added. [Ru]-DNA solutions were allowed to incubate for 5 min before the fluorescence emission spectra were recorded. The intrinsic binding constant (K_b) of each Ru (II) complexes to CT DNA was obtained by the following equations:

$$(F_a\text{-}F_f)/(F_b\text{-}F_f) = (b\text{-}(b^2\text{-}2K_b{}^2C_t[DNA]/s)^{1/2}/2K_bC_t \quad (2)$$

$$b = 1 + K_bC_t + K_b[DNA]/2s \quad (3)$$

where F_a, F_f, and F_b refer to the fluorescent intensities of the complex under a given DNA concentration, in the absence of DNA and in the fully DNA-bound form at 590 nm, respectively. C_t is the concentration of the Ru(II) complex. [DNA] is the DNA concentration in nucleotides and s is the binding site size of complexes with DNA in base pairs. Both the binding constant K_b and the binding site size (s) can be obtained by nonlinear least-squares fit analysis using equations (2) and (3).

Viscosity measurements were carried out using an Ubbelodhe viscometer maintained at a constant temperature at 25.0 (± 0.1) °C in a thermostatic bath. DNA samples approximately 200 base pairs in average length were prepared by sonication to minimize complexities arising from DNA flexibility [43]. Flow time was measured with a digital stopwatch, and each sample was measured three times, and an average flow time was calculated. Relative viscosities for DNA in the presence and absence of complex were calculated from the relation $\eta = (t - t^0)/t^0$, where t is the observed flow

time of the DNA-containing solution and t^0 is the flow time of buffer alone [44,45]. The change in the viscosity was presented as $(\eta/\eta_0)^{1/3}$ versus binding ratio [Ru]/[DNA] [46], where η is the viscosity of DNA solution in the presence of complexes and η_0 is the viscosity of DNA solution alone.

2.4. Cytotoxicity assay in vitro

Standard 3-(4,5-dimethylthiazole)-2,5-diphenyltetraazolium bromide (MTT) assay procedures were used [47,48]. Cells were placed in 96-well microassay culture plates (8×10^3 cells per well) and grown overnight at 37 °C in a 5% CO_2 incubator. The tested compounds were then added to the wells to achieve final concentrations ranging from 10^{-6} to 10^{-4} M. Control wells were prepared by addition of culture medium (100 μL). The plates were incubated at 37 °C in a 5% CO_2 incubator for 48 h. Upon completion of the incubation, stock MTT dye solution (20 μL, 5 mg·mL^{-1}) was added to each well. After 4 h, DMSO (100 μL) was added to solubilize the MTT formazan. The optical density of each well was then measured with a microplate spectrophotometer at a wavelength of 490 nm. The IC_{50} values were calculated by plotting the percentage viability versus concentration on a logarithmic graph and reading off the concentration at which 50% of cells remained viable relative to the control. Each experiment was repeated at least three times to obtain the mean values.

2.5. Apoptosis assessment by AO/EB staining

A549 cells were seeded onto chamber slides in six-well plates at a density of 2 ×

10^5 cells per well and incubated for 24 h. The cells were cultured in RPMI 1640 containing 10% of FBS and incubated at 37 ^oC in 5% CO_2. The medium was removed and replaced with medium (final DMSO concentration, 0.05% v/v) containing the complexes (4.5 μM) for 24 h. The medium was removed again, and the cells were washed with ice-cold phosphate buffer saline (PBS), and fixed with formalin (4%, w/v). Cell nuclei were counterstained with acridine orange (AO) and ethidium bromide (EB) (AO: 100 μg mL^{-1}, EB: 100 μgmL^{-1}) for 10 min. The cells were observed and imaged with a fluorescence microscope (Nikon, Yokohama, Japan) with excitation at 350 nm and emission at 460 nm.

2.6. Reactive oxygen species (ROS) levels studies

The levels of the ROS in A549 cells induced by the complexes were measured using the fluorescent dye 2′,7′-dichlorodihydrofluorescein diacetate (DCFH-DA). The cells were seeded in a 12-well plate with 2 × 10^5 cells each well, and incubated overnight. After being treated with different concentration of the complexes for 24 h, the cells were washed twice with cold PBS and subsequently prestained with DCFH-DA (10 mM) and incubated at 37 ^oC in the dark for 30 min. Afterward, the treated cells were washed two times with cold PBS, and stained with Hoechest 33342 for 20 min in the dark at 37 ^oC. Finally, the cells were washed twice with PBS, and then imaged and quantitatively analyzed using a confocal fluorescence microscope.

2.7. The change of mitochondrial membrane potential assay

A549 cells were inoculated at a density of 2 × 10^5 cells/well in 12-well plates and

incubated with or without different concentration of the complexes for 24 h at 37 ^{o}C, and then washed two times with PBS. Afterward, JC-1 dye (1 μg/mL) was added and incubated for 20 min in the dark at 37 ^{o}C. After being washed with PBS, the cells were suspended in PBS, and observed under an ImageXpress Micro XLS system.

2.8. Location assay of the complex in the mitochondria

A549 cells were placed in 12-well microassay culture plates (4×10^4 cells per well) and grown overnight at 37 ^{o}C in a 5% CO_2 incubator. 1.0 μM of the complexes were added to the wells at 37 ^{o}C in a 5% CO_2 incubator for 4 h and further co-incubated with MitoTracker® Deep Green FM (150 nM) at 37 ^{o}C for 0.5 h. Upon completion of the incubation, the wells were washed three times with ice-cold PBS. After discarding the culture medium, the cells were imaged under a fluorescence microscope.

2.9. Matrigel invasion assay

BD Matrigel invasion chamber was used to investigate cell invasion according to the manufacturer's instructions. A549 cells (4×10^4) in serum free medium containing different concentrations of the complexes were seeded into the top chamber of the two-chamber Matrigel system. RPMI 1640 medium (20% FBS) was added into the lower chamber. The cells were allowed to invade for 24 h. After incubation, non-invading cells were removed from the upper surface and cells on the lower surface were fixed with 4% paraformaldehyde and stained with 0.1% crystal

violet. The membranes were photographed and the invading cells were counted under a light microscope. The mean values from three independent assays were calculated.

3. Results and discussion

3.1. In vitro cytotoxicity assay

The MTT method was used to evaluate the antiproliferative activities of the Ru(II) complexes against A549, HepG-2, SGC-7901 and Hela cancer cells, in comparison with cisplatin as a positive control. The half maximal inhibitory concentration (IC_{50}) values are summarized in Table 1. As expectation, the ligand shows low cytotoxic activity (＞100 μM) against selected cancer cell lines. In addition, the complex **Ru(II)-4** displays excellent antitumor activity toward all selected cancer cell lines. Complexes **Ru(II)-1**, **Ru(II)-2** and **Ru(II)-3** have poor cytotoxic activity against HepG-2 cell lines. It is noteworthy that Ru(II) complexes exhibited well activity against A549 cells with IC_{50} values of 9.3 ± 1.2 (**Ru(II)-1**), 12.1 ± 1.6 (**Ru(II)-2**), 10.3 ± 1.6 (**Ru(II)-3**) and 8.9 ± 1.2 (**Ru(II)-4**) μM, respectively, which are similar to the anticancer activity of cisplatin. Thus, the complexes exhibits higher cytotoxicity than ruthenium(II) complexes $[Ru(ttbpy)_2(MHPIP)](ClO_4)_2$ (IC_{50} = 33.8 ± 4.0 μM) [49] and $[Ru(bpy)_2(HDPIP)](ClO_4)_2$ (13.3 ± 1.1 μM) [50]. Therefore, we conclude when BTPIP bonded ruthenium(II) to form complexes, the cytotoxic activity can be greatly increased, and the Ru(II) complexes reveals high inhibitory effect on the cell growth in A549, SGC-7901 and Hela cells and may be used as a potent broad-spectrum anticancer drugs. Because all the Ru(II) complexes is sensitive to

A549 cells, this cells were selected for the following experiments.

3.2. Apoptosis assay with AO/EB and Annex V/PI double staining methods

Apoptosis induced by the Ru(II) complexes in A549 cells was investigated using both qualitative and quantitative methods. The morphological changes of A549 cells were obtained using AO/EB doubled staining methods [51]. As shown in Fig. 1, in the control (a), the living cells show bright green with intact cell nuclei. After the treatment of A549 cells with 4.5 μM of complexes **Ru(II)-1**, **Ru(II)-2**, **Ru(II)-3** and **Ru(II)-4** for 24 h, the A549 cells with apoptotic features such as nuclear shrinkage, cell blebbing and chromatin condensation were detected (Fig. 1 b, c, d, e), The results revealed the Ru(II) complexes triggered apoptosis in A549 cells.

To further quantitatively analyze the extent of the four Ru(II) complexes on the apoptosis, flow cytometry technique was employed to investigate the percentage in the early and late apoptosis cells. As shown in Fig. 2, the total percentage of apoptotic cells (sum of early and late apoptosis cells) in A549 cells increased from 2.37% (a) to 10.68% (b), 11.73% (c), 7.08% (d) and 20.99% (e) after treatment with complexes **Ru(II)-1**, **Ru(II)-2**, **Ru(II)-3** and **Ru(II)-4**, respectively. From these observations, it can be deduced that the Ru(II) complexes induce obvious apoptosis in A549 cells and the apoptosis effects follow the order **Ru(II)-4 > Ru(II)-2 > Ru(II)-1 > Ru(II)-3**.

3.3. Intracellular reactive oxygen species levels determination

ROS can affect mitochondrial membrane potential and then cause a chain of

mitochondria-associated events, such as apoptosis [52]. Therefore, it was of interest to investigate whether the ruthenium(II) complexes would lead to increased ROS generation. Herein, the ROS levels were investigated using a DCFH-DA (2′,7′-dichlorodihydrofluorescein diacetate) probe. It is well known that DCFH-DA is cleaved by intracellular esterase into its non-fluorescent form (DCFH), and DCFH is oxidized by ROS to generate a fluorescent product DCF (dichlorofluorescein). Consequently, the fluorescence intensity of DCF can reflect the content of intracellular ROS [53]. A549 cells were treated with 4.5 μM of different Ru(II) complexes for 24 h, stained with DCFH-DA and detected by ImageXpress Micro XLS system. As described in Fig. 3, in the control (a), no obvious fluorescence was observed. However, after A549 cells were treated with Rosup (positive control, b), **Ru(II)-1** (4.5 μM, c), **Ru(II)-2** (4.5 μM, d), **Ru(II)-3** (4.5 μM, e) and **Ru(II)-4** (4.5 μM, f) for 24 h, the obvious green fluorescence were found, which indicates that the Ru(II) complexes can increase the contents of ROS. To quantitatively investigate the effect of concentration of the Ru(II) complexes on the ROS levels, The DCF fluorescent intensity was tested and depicted in Fig. 4. In the control, the fluorescent intensity of DCF is 1.9. However, A549 cells were treated with 9.0 μM of complexes **Ru(II)-1**, **Ru(II)-2**, **Ru(II)-3** and **Ru(II)-4**, the fluorescent intensities are 35.4, 12.7, 20.0 and 57.6, respectively. Compared the effect with the control, the fluorescent intensities of DCF grow 18.6, 6.7, 10.5, and 30.3 times than the original. Furthermore, the content of ROS shows a dose-dependent manner.

ROS include superoxide anion ($O_2^{\bullet-}$), hydrogen peroxide (H_2O_2) and nitric oxide

(NO), etc [54]. Among them, superoxide anion plays a vital role in cancer cell death [55]. Subsequently, the level of superoxide anion was investigated by DHE assay. The non-fluorescent DHE could enter into cells freely and interact with superoxide anion to form the membrane-impermeant ethidium cation, which becomes fluorescent upon intercalating DNA, thus the fluorescence intensity of ethidium-DNA can indicate the level of intracellular $O_2^{\bullet-}$[56] As described in Fig. 5, Comparing with the control (a), the treatment of A549 cells with complexes **Ru(II)-1** (b), **Ru(II)-2** (c), **Ru(II)-3** (d) and **Ru(II)-4** (e) led to an obvious increase in the red fluorescent points. In addition, the red fluorescence intensity was determined by ImageXpress Micro XLS system and is depicted in Fig. 6, all the ruthenium(II) complexes can enhance the levels of $O_2^{\bullet-}$ in a dose-dependent manner.

The content of nitric oxide is closely related to cancer cells apoptosis and necrosis [57]. 3-Amino, 4-aminomethyl-2′,7′-difluorescein, diacetate (DAF-FM DA) was used as a fluorescent indicator of intracellular nitric oxide (NO). As described in Fig. 7, treatment of A549 cells with 4.5 μM of **Ru(II)-1** (b), **Ru(II)-2** (c), **Ru(II)-3** (d), and **Ru(II)-4** (e) for 24 h, more bright green fluorescent points were detected compared with the control (a), which confirms that the levels of NO was increased. The fluorescence intensity of DAF-FMDA was tested using ImageXpress Micro XLS system. As described in Fig. 8, exposure of A549 cells to 4.5 and 9.0 μM of Ru(II) complexes led to an remarkable increase in green fluorescence intensity of 4.96 and 10.04 times for **Ru(II)-1**, 3.43 and 7.53 times for **Ru(II)-2**, 4.18 and 9.03 times for **Ru(II)-3**, 4.28 and 11.76 times for **Ru(II)-4** than that of control, respectively. This

further confirms that the Ru(II) complexes can increase the content of nitric oxide. Furthermore, the level of NO shows a dose-dependent manner.

3.4. Location assay of the complexes and mitochondrial membrane potential (MMP) analysis

Mitochondria play a vital role in a series of cellular processes, deciding the fate of a cell by controlling the process of apoptosis [58]. In order to research the location of the ruthenium(II) polypyridyl complexes in the mitochondrial, Mito Tracker® Deep Green FM (ThermoFisher, 100 nM) was used as a green fluorescent dye. As shown in Fig. 9, in the control, the mitochondria were stained in bright green. The treatment of A549 cells with 1.0 μM of **Ru(II)-1**, **Ru(II)-2**, **Ru(II)-3** and **Ru(II)-4** for 4 h, the Ru(II) complexes emits red fluorescence. The merge of the green and red fluorescence reveals that the Ru(II) complexes could reach the cytoplasm through the cell membrane and accumulate in the mitochondria. To further explore the possible anticancer mechanism, we studied the effects of Ru(II) complexes on the mitochondrial membrane potential (MMP) of A549 cells using JC-1 (5′,6′,6′-tetrachlore-1,1′,3,3′-tetraethylbenzimidazolylcarbocyanine iodide). The accumulation of JC-1 in mitochondria is potential-dependent, and it is demonstrated by a shift in its fluorescence emission from red (~590 nm) to green (~525 nm) [59]. Image of A549 cells obtained using fluorescence microscope. As depicted in Fig. 10, in the control (a), JC-1 emits red fluorescence corresponding to high MMP. After A549 cells were exposed to CCCP (carbonylcyanide-m-chlorophenylhydrazone, b,

positive control), **Ru(II)-1** (4.5 μM, c), **Ru(II)-2** (4.5 μM, d), **Ru(II)-3** (4.5 μM, e) and **Ru(II)-4** (4.5 μM, f) for 24 h, JC-1 emits green fluorescence corresponding to low MMP. These findings suggest that treatment with Ru(II) complexes causes a remarkable decrease of MMP which is evidenced by an opposite fluorescence emission shift from red to green [60]. Furthermore, the ratio of red/green fluorescent intensity was also detected by ImageXpress Micro XLS system. As shown in Fig. 11, in the control and in the presence of CCCP, the ratios of red/green are 0.94 and 0.49, respectively. Treatment of A549 cells with different concentrations of Ru(II) complexes led to an decrease of the ratio of red/green. It is further proved that the Ru(II) complexes can induce the decrease of membrane potential of mitochondria.

3.5. Transwell cell migration and invasion assay

The migration and invasion are the vital factors in the process of cancer metastasis [61-63]. According to the observations above, designed Ru(II) complexes can induce apoptosis and effectively inhibit the A549 cells growth. Therefore, it is reasonable to deduce that Ru(II) complexes may have the capability to inhibit the migration of A549 cells. We carried out Boyden chamber invasion assay to confirm the effect of Ru(II) complexes on the invasive ability of A549 cells. As seen in Fig. 12, invasive ability of A549 cells was reduced by the treatment with 4.5 μM of different Ru(II) complexes (b, c, d, e) with the control (a). Then, the percentage of Ru(II) complexes inhibiting the cell invasion is calculated in Fig. 13. A549 cells were treated with 9.0 μM of complexes **Ru(II)-1**, **Ru(II)-2**, **Ru(II)-3** and **Ru(II)-4** for 24 h, and the

percentage of inhibiting the cell invasion reaches 63.4%, 51.9%, 54.1% and 65.7%, respectively. Besides, it is clear that the Ru(II) complexes inhibited cell invasion with a dose-dependent manner.

3.6. Cell cycle arrest studies

The inhibition of cell viability by anticancer drugs can result from cycle cell arrest, induction of apoptosis, or a combined action of these two mechanisms [64]. We therefore investigated whether target Ru(II) complexes altered the cell cycle of A549 cells and induced apoptosis of A549 cells using flow cytometric analyses. As seen in Fig. 14, in the control (a), the percentage in the cell cycle at S phase is 24.78%. Treatment of A549 cells with different Ru(II) complexes, the percentages in the at S phase are 38.83% (b), 41.24% (c), 34.58% (d) and 40.73% (e), respectively, An obvious increase of 14.05% for **Ru(II)-1**, 16.46% for **Ru(II)-2**, 9.80% for **Ru(II)-3** and 15.95% for **Ru(II)-4** in the percentage at S phase was detected, at the same time, a reduction of 10.82% for **Ru(II)-1**, 15.54% for **Ru(II)-2**, 8.39% for **Ru(II)-3** and 14.31% for **Ru(II)-4** in the cell at G_0/G_1 phase compared with the control were discovered. These results demonstrate that the antiproliferative mechanism induced by Ru(II) complexes on A549 cells was a S phase arrest. In addition, a population of sub-G_1-phase cells (Apo), the characteristic of apoptosis, was increased dramatically with the incubation of Ru(II) complexes.

3.7. Complexes-CT DNA binding studies

Electronic absorption spectroscopy is the effective way to investigate the binding mode of complexes with DNA by testing changes in absorption intensity and position of the bands [65]. The electronic absorption spectra of complexes **Ru(II)-1**, **Ru(II)-2**, **Ru(II)-3** and **Ru(II)-4** mainly consist one or two resolved bands in the range of 300-600 nm. Fig. S1 shows spectra obtained at increasing amounts of CT DNA (0.75 μM) to **Ru(II)-1** (5.0 μM), **Ru(II)-2** (5.0 μM), **Ru(II)-3** (5.0 μM) and **Ru(II)-4** (5.0 μM) (10 μL of CT DNA was added to corresponding solutions each time, see the Supporting Information for details). As the CT DNA concentration increased, the MLCT (metal-to-ligand charge transfer) bonds of **Ru(II)-1** at 467 nm, **Ru(II)-2** at 465 nm, **Ru(II)-3** at 476 nm and **Ru(II)-4** at 479 nm exhibit hypochromism of about 26.4%, 26.6%, 16.2%, 21.0%, and bathochromism of 5, 6, 2 and 2 nm, respectively. The K_b values of **Ru(II)-1**, **Ru(II)-2**, **Ru(II)-3** and **Ru(II)-4** are 1.2×10^6 M^{-1}, 3.81×10^6 M^{-1}, 1.09×10^6 M^{-1} and 5.41×10^5 M^{-1}, respectively, which are less than that of the complexes $[Ru(phen)_2(dppz)]^{2+}$ (5.1×10^6 M^{-1}) [66] and $[Ru(dmb)_2(dppz)]^{2+}$ (4.5×10^6 M^{-1}) [67], but were higher than that of complexes $[Ru(phen)_2bppp](ClO_4)_2$ (5.51×10^5 M^{-1}) [68] and $[Ru(bpy)_2(ppd)]^{2+}$, (1.3×10^6) [69].

Fluorescence emission spectra are the most common and most effective way to analyze complex-nucleic acid interactions [70]. The emission intensities of the **Ru(II)-1**, **Ru(II)-2**, **Ru(II)-3** and **Ru(II)-4** from their MLCT excited states upon excitation at 594, 577 and 604 nm were found to depend on CT DNA concentration. As shown in Fig. S2, the emission intensities of Ru(II) complexes grow to 1.9 (**Ru(II)-1**), 2.4 (**Ru(II)-2)** and 1.4 (**Ru(II)-3**) times larger than the original,

respectively. The results indicates that target Ru(II) complexes can effectively interact with CT DNA, and the Ru(II) complexes can be protected efficiently by the hydrophobic environment inside the CT DNA helix [71]. The intrinsic binding constants K_b of **Ru(II)-1**, **Ru(II)-2** and **Ru(II)-3** to CT DNA calculated from equations (eq 2) and equations (eq 3) are 7.68×10^5 M^{-1}, 8.91×10^5 M^{-1}, 5.56×10^5 M^{-1} respectively, which are higher than that of the complexes *Δ*-$[Ru(bpy)_2PBIP]^{2+}$ (4.1×10^5 M^{-1}) and *Λ*-$[Ru(bpy)_2PBIP]^{2+}$ (2.6×10^5 M^{-1}) [72].

To further confirm the mode of designed Ru(II) complexes with CT DNA, viscosity measurements of CT DNA solutions were carried out in the presence and absence of these complexes [13]. Viscosity of CT DNA is sensitive to its length. Compounds are expected to elongate the double helix to accommodate the ligands in between the base leading to an increase in the viscosity of CT DNA [73]. The effects of target Ru(II) complexes **Ru(II)-1**, **Ru(II)-2**, **Ru(II)-3** and **Ru(II)-4** on the viscosity of CT DNA were seen in Fig. 15. On increasing the amount of Ru(II) complexes, the relative viscosity of CT DNA solution increases steadily. The increased degree of viscosity, which may depend on its affinity to CT DNA follows order of **Ru(II)-2** > **Ru(II)-1** > **Ru(II)-3** > **Ru(II)-4**. These results indicated that the designed Ru(II) complexes bind CT DNA through a classical intercalation model, which was consistent with binding constants.

4. Conclusions

A novel ligand BTPIP and its four Ru(II) polypyridyl complexes

$[Ru(bpy)_2(BTPIP)](ClO_4)_2$ (**Ru(II)-1**), $[Ru(phen)_2(BTPIP)](ClO_4)_2$ (**Ru(II)-2**), $[Ru(dmb)_2(BTPIP)](ClO_4)_2$ (**Ru(II)-3**) and $[Ru(dmp)_2(BTPIP)](ClO_4)_2$ (**Ru(II)-4**) were synthesized and characterized. Designed Ru(II) polypyridyl complexes interact with CT DNA most probably by intercalative binding mode. They exhibited good activity against selected cancer cells, especially A549 cells. In addition, AO/EB and Annex V/PI staining assay demonstrates that the complexes can obviously induce the apoptosis of A549 cells. Detailed studies on the Ru(II) complexes, suggest that they localizes mainly in the mitochondria, causing a decrease in mitochondrial membrane potential and ROS release into cytoplasm, which further induced mitochondria dysfunction and the onset of apoptotic cell death mechanism. Further anticancer mechanistic studies reveal that these complexes can significantly inhibit cell invasion and induce cell cycle arrest of A549 cells at S phase. According to the results of these experiments, we suggest that designed Ru(II) complexes may be a candidate for further evaluation as a chemopreventive and chemotherapeutic agent for human lung cancer.

Acknowledgements

The authors thank the Guangxi Natural Science Foundation (2018GXNSFBA050024), the Ph. D. Scientific Research Foundation of Guilin University of Technology, and Key Laboratory of Electrochemical and Magneto-chemical Function Materials.

References

[1] B. Wang, Z. Wang, F. Ai, W.K. Tang, G. Zhu, A monofunctional platinum(II)-based anticancer agent from a salicylanilide derivative: Synthesis, antiproliferative activity, and transcription inhibition, J. Inorg. Biochem. 142 (2015) 118-125.

[2] X. Wang, Z. Guo, Targeting and delivery of platinum-based anticancer drugs, Chem. Soc. Rev. 42 (2013) 202-224.

[3] W.J. Rieter, K. M. Pott, K. M.L. Taylor, W. Lin, Nanoscale Coordination Polymers for Platinum-Based Anticancer Drug Delivery, J. Am. Chem. Soc. 130 (2008) 11584-11585.

[4] C. Brauckmann, C.A. Wehe, M. Kieshauer, C. Lanvers-Kaminsky, M. Sperling, U. Karst, The interaction of platinum-based drugs with native biologically relevant proteins, Anal. Bioanal. Chem. 405 (2013) 1855-1864.

[5] T. Sun, W. Cui, M. Yan, G. Qin, W. Guo, H. Gu, S. Liu, Q. Wu, Target Delivery of a Novel Antitumor Organoplatinum(IV) - Substituted Polyoxometalate Complex for Safer and More Effective Colorectal Cancer Therapy In Vivo, Adv. Mater. 28 (2016) 7397-7404.

[6] E. Wong, C.M. Giandomenico, Current Status of Platinum-Based Antitumor Drugs, Chem. Rev. 99 (1999) 2451-2466.

[7] U. Kalinowska-Lis, J. Ochocki, K. Matlawska-Wasowska, Trans geometry in platinum antitumor complexes, Coordin. Chem. Rev. 252 (2008) 1328-1345.

[8] M. Imran, W. Aybu, I.S. Butler, Z.U. Rehman, Photoactivated platinum-based

anticancer drugs, Coordin. Chem. Rev. 376 (2018) 405-429.

[9] J. Qi, S. Liang, Y. Gou, Z. Zhang, Z. Zhou, F. Yang, H. Liang, Synthesis of four binuclear copper (II) complexes: Structure, anticancer properties and anticancer mechanism, Eur. J. Med. Chem. 96 (2015) 360-368.

[10] Z. Yu, M. Han, J. Cowan, Toward the Design of a Catalytic Metallodrug: Selective Cleavage of G-Quadruplex Telomeric DNA by an Anticancer Copper-Acridine-ATCUN Complex, Angew. Chem. Int. Ed. 53 (2014) 1901-1905.

[11] Y.-Y. Qi, Q. Gan, Y.-X. Liu, Y.-H. Xiong, Z.-W. Mao, X.-Y. Le, Two new Cu(II) dipeptide complexes based on 5-methyl-2-(2′-pyridyl)benzimidazole as potential antimicrobial and anticancer drugs: Special exploration of their possible anticancer mechanism, Eur. J. Med. Chem. 154 (2018) 220-232.

[12] L. Xie, Z. Luo, Z. Zhao, T. Chen, Anticancer and antiangiogenic iron (II) complexes that target thioredoxin reductase to trigger cancer cell apoptosis, J. Med. Chem. 60 (2017) 202-214.

[13] G. Jiang, X. Zheng, J.H. Yao, B. Han, W. Li, J. Wang, H. Huang, Y. Liu, Ruthenium (II) polypyridyl complexes induce BEL-7402 cell apoptosis by ROS-mediated mitochondrial pathway, J. Inorg. Biochem. 141 (2014) 170-179.

[14] J. Sun, W.X. Chen, X.D. Song, S.F. He, J.X. Chen, J. Mei, X.X. Zhu, T. Wu, Synthesis, characterization and anticancer activity of two Ru (II) polypyridyl complexes $[Ru(dpq)_2L](PF_6)_2$ (L= maip, paip), Anti-Cancer Agent. Me. 18 (2018) 110-120.

[15] L. Zeng, P. Gupta, Y. Chen, E. Wang, L. Ji, H. Chao, Z.-S. Chen, The

development of anticancer ruthenium(II) complexes: from single molecule compounds to nanomaterials, Chem. Soc. Rev. 46 (2017) 5771-5804.

[16] C. Li, K.-W. Ip, W.-L. Man, D. Song, M.-L. He, S.-M. Yiu, T.-C. Lau, G. Zhu, Cytotoxic (Salen) ruthenium(III) Anticancer Complexes Exhibit Different Modes of Cell Death Directed by Axial Ligands, Chem. Sci. 8 (2017) 6865-6870.

[17] C. T, S. Lai, S. Wu, S. Hu, L. Zhou, Y. Chen, M. Wang, Y. Zhu, W. Lian, W. Peng, L. Ji, A. Xu, Nuclear Permeable Ruthenium(II) *β*-Carboline Complexes Induce Autophagy To Antagonize Mitochondrial-Mediated Apoptosis, J. Med. Chem. 53 (2010) 7613-7624.

[18] A. Martinez, T. Carreon, E. Iniguez, A. Anzellotti, A. Sánche, M. Tyan, A. Sattler, L. Herrera, R. A. Maldonado, R. A. Sánchez-Delgado, Searching for New Chemotherapies for Tropical Diseases: Ruthenium-Clotrimazole Complexes Display High in Vitro Activity against Leishmania major and Trypanosoma cruzi and Low Toxicity toward Normal Mammalian Cells, J. Med. Chem. 55 (2012) 3867-3877.

[19] B.S. Howerton, D.K. Heidary, E.C. Glazer, Strained Ruthenium Complexes Are Potent Light-Activated Anticancer Agents, J. Am. Chem. Soc. 134 (2012) 8324-8327.

[20] T. Mede, M. Jäger, U.S.Schubert, “Chemistry-on-the-complex”: functional Ru II polypyridyl-type sensitizers as divergent building blocks, Chem. Soc. Rev. 47 (2018) 7577-7627.

[21] J. Yellol, S.A. Pérez, A. Buceta, C. Yellol, A. Donaire, P. Szumlas, P.J. Bednarski,

G. Makhloufi, C. Janiak, A. Esspinosa, J. Ruiz, Novel C, N-Cyclometalated Benzimidazole Ruthenium(II) and Iridium(III) Complexes as Antitumor and Antiangiogenic Agents: A Structure-Activity Relationship Study, J. Med. Chem. 58 (2015) 7310-7327.

[22] A. Castonguay, C. Doucet, M. Juhas, D. Maysinger, New ruthenium (II)-letrozole complexes as anticancer therapeutics, J. Med. Chem. 55 (2012) 8799-8806.

[23] P. Florindo, D.M. Pereira, P.M. Borralho, C.M.P. Rodrigues, M.F.M. Piedade, A. C. Fernandes, Cyclopentadienyl-Ruthenium(II) and Iron(II) Organometallic Compounds with Carbohydrate Derivative Ligands as Good Colorectal Anticancer Agents, J. Med. Chem. 58 (2015) 4339-4347.

[24] L. Zeng, Y. Chen, J. Liu, H. Huang, R. Guan, L. Ji, H. Cao, Ruthenium (II) complexes with 2-phenylimidazo [4,5-f][1,10] phenanthroline derivatives that strongly combat cisplatin-resistant tumor cells, Sci. Rep. 6 (2016) 19449.

[25] J. Du, Y. Kang, Y. Zhao, W. Zheng, Y. Zhang, Y. Lin, Z.Y. Wang, Y.Y. Wang, ,Q. Luo, K. Wu, F.Y. Wang, Synthesis, Characterization, and in Vitro Antitumor Activity of Ruthenium(II) Polypyridyl Complexes Tethering EGFR-Inhibiting 4-Anilinoquinazolines, Inorg. Chem. 55 (2016) 4595-4605.

[26] P. Elumalai, Y.J. Jeong, D.W. Park, D.H. Kim, H. Kim, S.C. Kang, K.W. Chi, Antitumor and biological investigation of doubly cyclometalated ruthenium(II) organometallics derived from benzimidazolyl derivatives, Dalton Trans. 45 (2016) 6667-6673.

[27] T. Lazarević, A. Rilak, Ž.D. Bugarčić, Ž.D. Bugarčić, Platinum, palladium, gold

and ruthenium complexes as anticancer agents: Current clinical uses, cytotoxicity studies and future perspectives, Eur. J. Med. Chem. 142 (2017) 8-31.

[28] L. Li, Y.-S. Wong, T. Chen, C. Fan, W. Zheng, Ruthenium complexes containing bis-benzimidazole derivatives as a new class of apoptosis inducers, Dalton Trans. 41 (2012) 1138-1141.

[29] T. Chen, Y. Liu, W.-J. Zheng, J. Liu, Y.-S. Wong, Ruthenium polypyridyl complexes that induce mitochondria-mediated apoptosis in cancer cells, Inorg. Chem. 49 (2010) 6366-6368.

[30] A. Castonguay, C. Doucet, M. Juhas, D. Maysinger, New ruthenium(II)-letrozole complexes as anticancer therapeutics, J. Med. Chem. 55 (2012) 8799-8806.

[31] J. Liu, Y. Chen, G. Li, P. Zhang, C. Jin, L. Zeng, L. Ji, H. Chao, Ruthenium(II) polypyridyl complexes as mitochondria-targeted two-photon photodynamic anticancer agents, Biomaterials 56 (2015) 140-153.

[32] B. Tang, D. Wan, S.-H. Lai, H.-H. Yang, C. Zhang, X.-Z. Wang, C.-C. Zeng, Y.-J. Liu, Design, synthesis and evaluation of anticancer activity of ruthenium (II) polypyridyl complexes, J. Inorg. Biochem. 173 (2017) 93-104.

[33] J. Cheong, M. Zaffagni, L. Chung, Y. Xu, Y. Wang, F.E. Jernigan, B.R. Zetter, L. Sun, Synthesis and anticancer activity of novel water soluble benzimidazole carbamates, Eur. J. Med. Chem. 144 (2018), 372-385.

[34] H.I. Gul, C. Yamali, H. Sakagami, A. Angeli, J. Leitans, A. Kazaks, K. Tars, D.O. Ozgun, C.T. Supuran, New anticancer drug candidates sulfonamides as selective hCA IX or hCA XII inhibitors, Bioorgan. Chem. 77 (2018) 411-419.

[35] M. Jeon, J. Park, P. Dey, Y. Oh, H. Oh, S. Han, S.H. Um, H.S. Kim, N.K. Mishra, I.S. Kim, Site-Selective Rhodium(III)-Catalyzed C-H Amination of 7-Azaindoles with Anthranils: Synthesis and Anticancer Evaluation, Adv. Synth. Catal. 359 (2017) 3471-3478.

[36] J.F.D. Oliveira, A.L.D. Silva, D.B. Vendramini-Costa, C.A.D.C. Amorim, J.F. Campos, A.G. Ribeiro, R.O.D. Moura, J.L. Neves, A.L.T.G. Ruiz, J.E.D. Carvalho, M.D.C.A.D. Lima, Synthesis of thiophene-thiosemicarbazone derivatives and evaluation of their in vitro and in vivo antitumor activities, Eur. J. Med. Chem. 104 (2015) 148-156.

[37] K.C. Gulipalli, S. Bodige, P. Ravula, S. Endoori, G.R. Vanaja, S. Babu, N.S. Chandra, N. Seelam, Bioorg. Design, synthesis, in silico and in vitro evaluation of thiophene derivatives: A potent tyrosine phosphatase 1B inhibitor and anticancer activity, Med. Chem. Lett. 27 (2017) 3558-3564.

[38] Y. Tang, J. Zhang, S. Zhang, R. Geng, C. Zhou, Synthesis and characterization of thiophene-derived amido bis-nitrogen mustard and its antimicrobial and anticancer activities, Chin. J. Chem. 30 (2012) 1831-1840.

[39] L. Perdisatt, S. Moqadasi, L. O′Neill, G, Hessman, A. Ghion, M.Q.M. Warraich, A. Casey, C. O′Connor, Synthesis, characterisation and DNA intercalation studies of regioisomers of ruthenium (II) polypyridyl complexes, J. Inorg. Biochem. 182 (2018) 71-82.

[40] J. Marmur, A procedure for the isolation of deoxyribonucleic acid from micro-organisms, J. Mol. Biol. 3 (1961) 208-218.

[41] M.E. Reichmann, S.A. Rice, C.A. Thomas, P. Doty, A further examination of the molecular weight and size of desoxypentose nucleic acid, J. Am. Chem. Soc. 76 (1954) 3047-3053.

[42] A. Wolf, G.H. Shimer, T. Meehan, Polycyclic aromatic hydrocarbons physically intercalate into duplex regions of denatured DNA, Biochemistry. 26 (1987) 6392-6396.

[43] J.B. Chaires, N. Dattagupta, D.M. Crothers, Studies on interaction of anthracycline antibiotics and deoxyribonucleic acid: equilibrium binding studies on the interaction of daunomycin with deoxyribonucleic acid, Biochemistry. 21 (1982) 3933-3940.

[44] S. Satyanarayana, J.C. Dabrowiak, J.B. Chaires, Tris (phenanthroline) ruthenium (II) enantiomer interactions with DNA: mode and specificity of binding, Biochemistry. 32 (1993) 2573-2584.

[45] S. Satyanaryana, J.C. Dabrowial, J.B. Chaires, Neither .DELTA.- nor .LAMBDA.-tris(phenanthroline)ruthenium(II) binds to DNA by classical intercalation, Biochemistry. 31 (1992) 9319-9324.

[46] G. Cohen, H. Eisenberg, Viscosity and sedimentation study of sonicated DNA-proflavine complexes, Biopolymers. 8 (1969) 45-55.

[47] S.D.A. Abel, S.K. Baird, Honey is cytotoxic towards prostate cancer cells but interacts with the MTT reagent: Considerations for the choice of cell viability assay, Food. Chem. 241 (2018) 70-78.

[48] B. Kadriye, T. Yagmur, C. Zerrin, A. Oge, A. Filiz, Cytotoxic and genotoxic

effects of $[Ru(phi)_3]^{2+}$ evaluated by Ames/Salmonella and MTT methods, Eur. J. Med. Chem. 44 (2009) 2601-2605.

[49] D. Wan, B. Tang, Y.-J. Wang, B.-H. Guo, H. Yin, Q.-Y. Yi, Y.-J. Liu, Synthesis and anticancer properties of ruthenium (II) complexes as potent apoptosis inducers through mitochondrial disruption, Eur. J. Med. Chem. 139 (2017) 180-190

[50] B.-J. Han, G.-B Jiang, J. Wang, W. Li, H.-L. Huang, Y.-J. Liu, The studies on bioactivity in vitro of ruthenium(II) polypyridyl complexes towards human lung carcinoma A549 cells, RSC Adv. 4 (2014) 40899-40906.

[51] J.R. Nakkala, R. Mata, K. Raja, V.K. Chandra, S.R. Sadras, Evaluation of in vitro anticancer activity of 1,8-Cineole-containing n-hexane extract of Callistemon citrinus (Curtis) Skeels plant and its apoptotic potential, Biomed. Pharmacoth. 93 (2017) 296-307.

[52] J.-C. Chen, Y. Zhang, X.-M. Jie, J. She, G.-Z. Dongye, Y. Zhong, Y.-Y. Deng, J. Wang, B.-Y. Guo, L.-M. Chen, Ruthenium (II) salicylate complexes inducing ROS-mediated apoptosis by targeting thioredoxin reductase, J. Inorg. Biochem. 193 (2019) 112-123.

[53] A. Armiñán, M. Palomino-Schätzlein, C. Deladriere, J.J. Arroyo-Crespo, S. Vicente-Ruiz, M.J. Vicent, A. Pineda-Lucena, Metabolomics facilitates the discrimination of the specific anti-cancer effects of free-and polymer-conjugated doxorubicin in breast cancer models, Biomaterials 162 (2018) 144-153.

[54] G.S. Shadel, T.L. Horvath, Mitochondrial ROS signaling in organismal homeostasis, Cell 163 (2015) 560-569.

[55] L. Diebold, N.S. Chandel, Mitochondrial ROS regulation of proliferating cells, Free Radic Biol Med 100 (2016) 86-93.

[56] H. He, D.W. Li, L.Y. Yang, L. Fu, X.J. Zhu, W.K. Wong, F.L. Jiang, Y. Liu, A novel bifunctional mitochondria-targeted anticancer agent with high selectivity for cancer cells, Sci. Rep. 5 (2015) 13543.

[57] S.R. Potje, Z. Chen, S.D.S. Oliveira, L.M. Bendhack, R.S.D. Silva, M.G. Bonini, C. Antoniali, R.D. Minshall, duces uncoupling and phosphorylation of endothelial nitric oxide synthase promoting oxidant production, Free Radic Biol Med 112 (2017) 587-596.

[58] Y. Xia, Q. Chen, X. Qin, D. Sun, J. Zhang, J. Liu, Studies of ruthenium (ii)-2, 2′-bisimidazole complexes on binding to G-quadruplex DNA and inducing apoptosis in HeLa cells, New. J. Chem. 37 (2013) 3706-3715.

[59] B. Peña, A. David, C. Pavani, M.S. Baptista, J.-P. Pellois, C. Turro, K.R. Dunbar, Cytotoxicity studies of cyclometallated ruthenium (II) compounds: New applications for ruthenium dyes, Organometallics 33 (2014) 1100-1103.

[60] J. Zhang, Q. YU, Q. Li, L. Yang, L. Chen, Y. Zhou, J. Liu, A ruthenium (II) complex capable of inducing and stabilizing bcl-2 G-quadruplex formation as a potential cancer inhibitor, J. Inorg. Biochem. 134 (2014) 1-11.

[61] C. Yang, Q. Xie, X. Zeng, N. Tao, Y. Xu, Y. Chen, J. Wang, L. Zhang, Novel hybrids of podophyllotoxin and formononetin inhibit the growth, migration and invasion of lung cancer cells, Bioorgan. Chem. 85 (2019) 445-454.

[62] W.Y. Zhang, Q.Y. Yi, Y.Y. Wang, F. Du, M. He, B. Tang, D. Wan, Y.J. Liu, H.L.

Huang, Photoinduced anticancer activity studies of iridium(III) complexes targeting mitochondria and tubules, Eur. J. Med. Chem. 151 (2018) 568-584.

[63] F.U. Rahman, M.Z. Bhatti, A. Ali, H.Q. Duong, Y. Zhang, B. Yang, S. Koppireddi, Y.J. Lin, H. Wang, Z.T. Li, D.W. Zhang, Homo-and heteroleptic Pt(II) complexes of ONN donor hydrazone and 4-picoline: A synthetic, structural and detailed mechanistic anticancer investigation, Eur. J. Med. Chem. 143 (2018) 1039-1052.

[64] Y. Alghamian, A.G. Abou, H. Murad, A. Madania, Effects of γ-radiation on cell growth, cell cycle and promoter methylation of 22 cell cycle genes in the 1321NI astrocytoma cell line, Adv Med Sci 62 (2017) 330-337.

[65] R.P. Paitandi, R.S. Singh, S. Mukhopadhyay, G. Sharma, B. Koch, P. Vishnoi, D.S. Pandey, Synthesis, characterization, DNA binding and cytotoxicity of fluoro-dipyrrin based arene ruthenium (II) complexes, Inorg. Chim. Acta. 454 (2017) 117-127.

[66] R.B. Nair, E.S. Teng, S.L. Kirkland, C.J. Murphy, Synthesis and DNA-Binding Properties of $[Ru(NH_3)_4dppz]^{2+}$, Inorg. Chem. 37 (1998) 139-141.

[67] S.R. Smith, G.A. Neyhart, W.A. Karlsbeck, H.H. Thorp, Electronic properties of aquapolypyridyl ruthenium complexes bound to DNA, New J. Chem. 18 (1994) 397-406.

[68] N. Deepika, C.S. Devi, Y.P. Kumar, K.L. Reddy, P.V. Reddy, D.A. Kumar, S.S. Singh, S. Satyanarayana, DNA-binding, cytotoxicity, cellular uptake, apoptosis and photocleavage studies of Ru (II) complexes, J Photochem Photobiol B Biol

160 (2016) 142-153.

[69] F. Gao, H. Chao, F. Zhou, Y.-X. Yuan, B. Peng, L.-N. Ji, DNA interactions of a functionalized ruthenium (II) mixed-polypyridyl complex $[Ru(bpy)_2ppd]^{2+}$, J. Inorg. Biochem. 100 (2006) 1487-1494.

[70] Y.P. Kumar, C.S. Devi, A. Srishailam, N. Deepika, V.R. Kumar, P.V. Reddy, K. Nagasuryaprasad, S.S. Singh, P. Nagababu, S. Satyanarayana, Studies on Photocleavage, DNA Binding, Cytotoxicity, and Docking Studies of Ruthenium (II) Mixed Ligand Complexes, J. Fluoresc. 26 (2016) 2119-2132.

[71] D. Lazić, A. Arsenijević, R. Puchta, Ž.D. Bugarčić, A. Rilak, DNA binding properties, histidine interaction and cytotoxicity studies of water soluble ruthenium (II) terpyridine complexes, Dalton Trans. 45 (2016) 4633-4646.

[72] W.-X. Hong, F. Huang, T. Huan, X. Xu, Q. Han, G. Wang, H. Xu, S. Duan, Y. Duan, X. Long, Y. Liu, Z. Hu, Comparative studies on DNA-binding and in vitro antitumor activity of enantiomeric ruthenium(II) complexes, J. Inorg. Biochem. 180 (2018) 54-60.

[73] A. Srishailam, Y.P. Kumar, P.V. Reddy, N. Nambigari, U. Vuruputuri, S.S. Singh, S. Satyanarayana, Cellular uptake, cytotoxicity, apoptosis, DNA-binding, photocleavage and molecular docking studies of ruthenium (II) polypyridyl complexes, J Photochem Photobiol B Biol 132 (2014) 111-123.

Captions for Schemes and Figures

Scheme 1 The synthetic route of ligand and ruthenium(II) complexes.

Fig. 1 Apoptosis in A549 cells (a) exposure to 4.5 μM of complexes **Ru(II)-1** (b), **Ru(II)-2** (c), **Ru(II)-3** (d) **Ru(II)-4** (e) for 24 h and the cells were stained with AO/EB.

Fig. 2 Apoptosis was assayed with Annex V/PI staining A549 cells (a) in the presence of **Ru(II)-1** (4.5 μM, b), **Ru(II)-2** (4.5 μM, c), **Ru(II)-3** (4.5 μM, d), and **Ru(II)-4** (4.5 μM, e) for 24 h.

Fig. 3 Intracellular ROS was detected in A549 cells (a) exposure to Rosup (b, positive control), 4.5 μM of **Ru(II)-1** (c), **Ru(II)-2** (d), **Ru(II)-3** (e) and **Ru(II)-4** (f) for 24 h.

Fig. 4 The DCF fluorescent intensity was determined after A549 cells treated with different concentration of the Ru(II) complexes for 24 h.

Fig. 5 The superoxide anion level was assayed after 24 h of A549 cells (a) with 4.5 μM of **Ru(II)-1** (b), **Ru(II)-2** (c), **Ru(II)-3** (d), **Ru(II)-4** (e) and the cells were stained with DHE.

Fig. 6 The DHE fluorescent intensity was determined after A549 cells treated with different concentration of the Ru(II) complexes for 24 h.

Fig. 7 The intracellular NO levels were detected after A549 cells (a) were exposed to 4.5 μM of **Ru(II)-1** (b), **Ru(II)-2** (c), **Ru(II)-3** (d), **Ru(II)-4** (e) for 24 h.

Fig. 8 The DAF-FMDA fluorescent intensity induced by the complexes was determined by ImageXpress Micro XLS system. $^{*}P < 0.05$ represents

significant differences compared with control.

Fig. 9 Location of complexes in the mitochondria in A549 cell exposure to 1.0 μM of Ru(II) complexes **Ru(II)-1**, **Ru(II)-2**, **Ru(II)-3**, **Ru(II)-4** for 4 h.

Fig. 10 The changes of mitochondrial membrane potential was studied after A549 cells (a) were treated with CCCP (b), 4.5 μM of complexes **Ru(II)-1** (c), **Ru(II)-2** (d), **Ru(II)-3** (e), **Ru(II)-4** (f) for 24 h and the cells were imaged under a fluorescent microscope.

Fig. 11 The ratio of the red/green fluorescent intensity was determined after A549 cells were treated with 4.5 and 9.0 μM of Ru(II) complexes for 24 h $^{*}P < 0.05$ represents significant differences compared with control. (For interpretation of the references to colour in this figure legend, the reader is referred to the web version of this article.)

Fig. 12 Microscope images of invading A549 cells (a) induced by 4.5 μM of **Ru(II)-1** (b), **Ru(II)-2** (c), **Ru(II)-3** (c), **Ru(II)-4** (c) for 24 h.

Fig. 13 Percentage of inhibiting invasion of A549 cells induced by different concentration of **Ru(II)-1**, **Ru(II)-2**, **Ru(II)-3**, **Ru(II)-4** for 24 h. $^{*}P < 0.05$ represents significant differences compared with control.

Fig. 14 The cell cycle arrest in A549 cells exposed to 4.5 μM of complexes **Ru(II)-1**, **Ru(II)-2**, **Ru(II)-3** and **Ru(II)-4** for 24 h.

Fig. 15 The effect of increasing the amounts of the **Ru(II)-1**, **Ru(II)-2**, **Ru(II)-3** and **Ru(II)-4** on the relative viscosity of CT DNA at 25 (± 0.1) ^{o}C. [DNA] = 0.25 mM.

Graphical abstract

DNA-binding behaviors of the complexes were investigated. Cytotoxicity was assessed by MTT method. Apoptosis, ROS, mitochondrial membrane potential, cell invasion and cell cycle arrest were studied.

Research highlights

- Four new ruthenium (II) complexes were synthesized and characterized.
- DNA-binding behaviors of the complexes were investigated.
- The anticancer activity of these complexes was evaluated by MTT method.
- The apoptosis was investigated by AO/EB staining method and flow cytometry.
- Reactive oxygen species and mitochondrial membrane potential were investigated.
- The cell cycle arrest and cell invasion were studied.

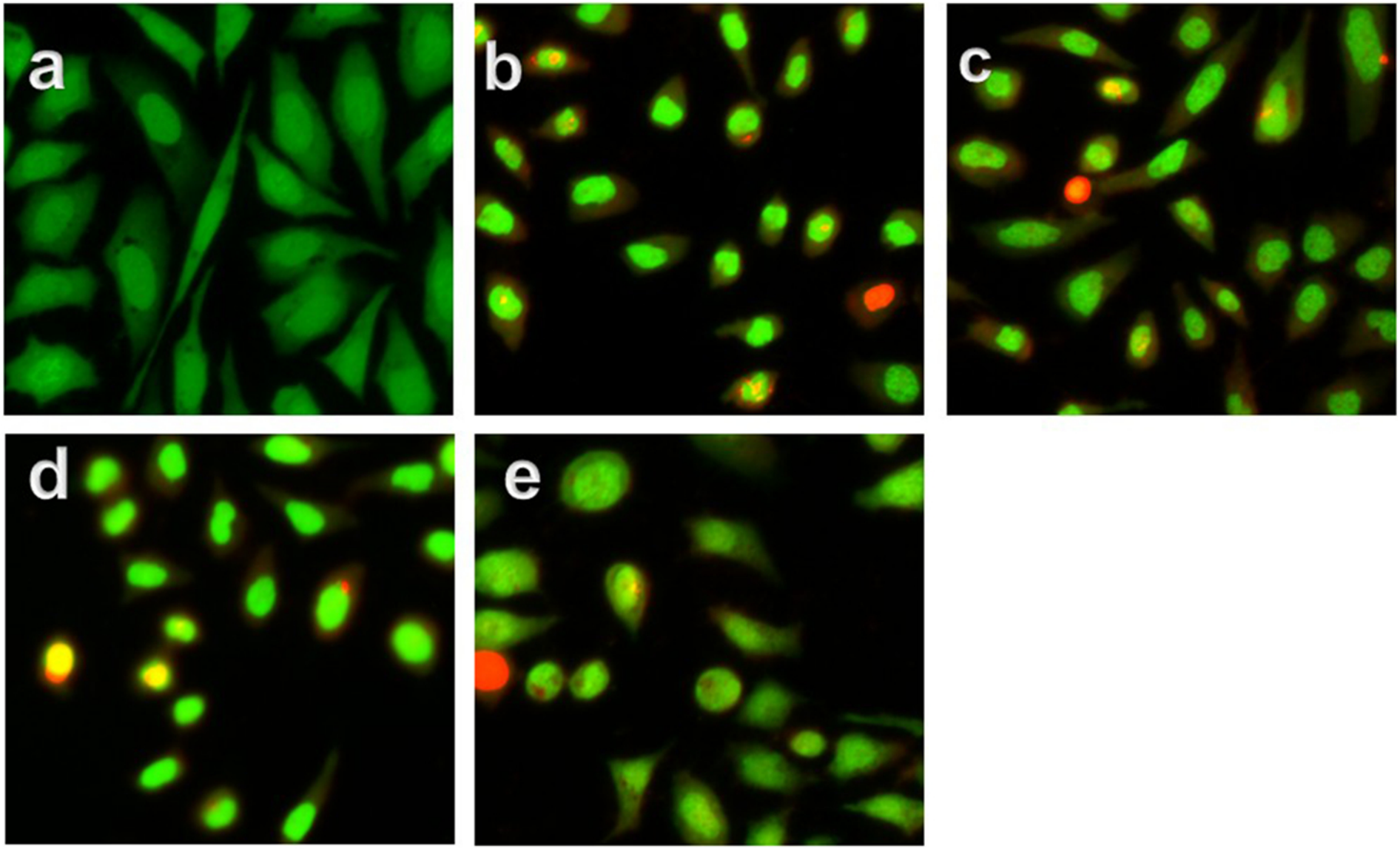

Figure 1

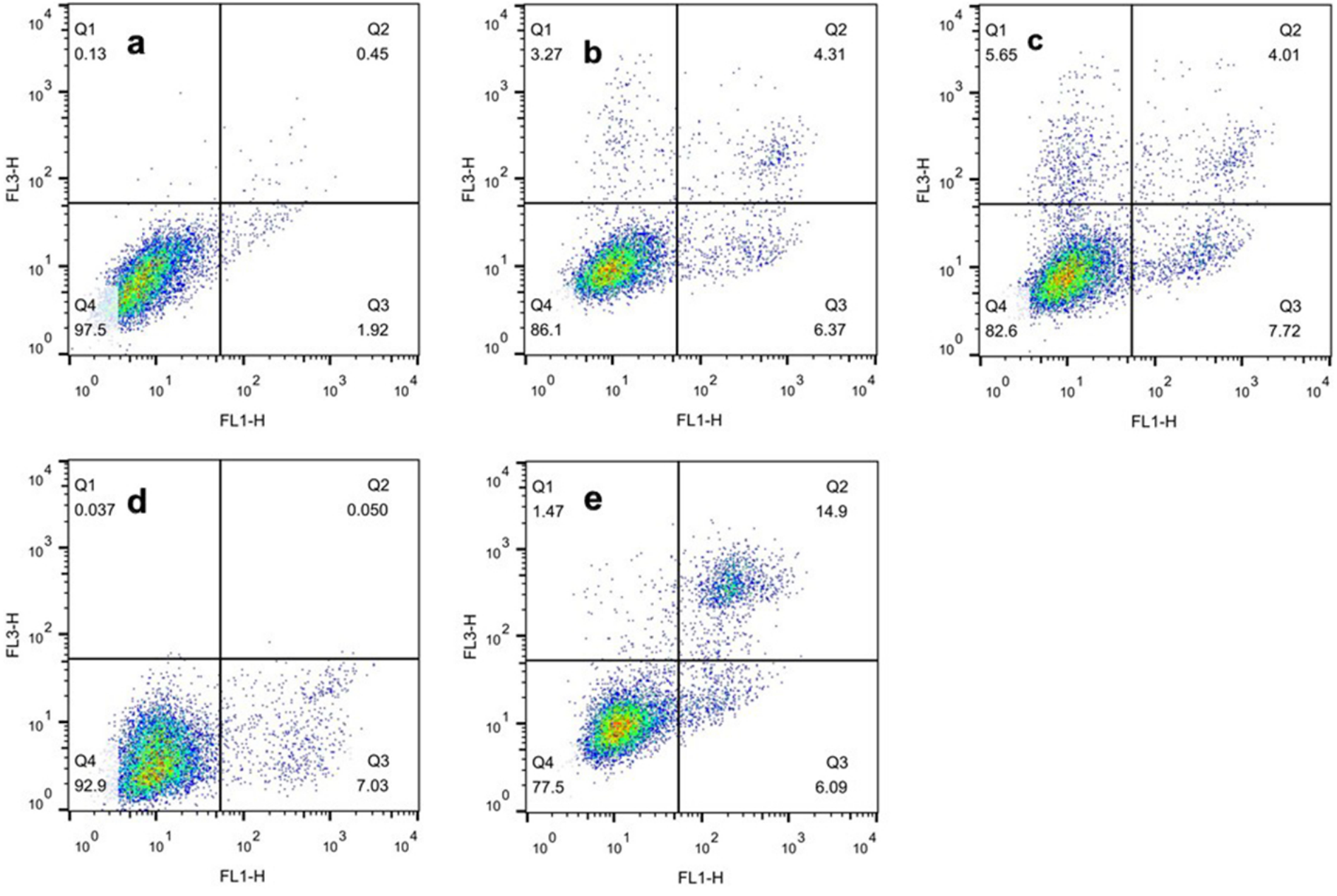
a
Q1
0.13
Q2
0.45
Q4
97.5
Q3
1.92
b
Q1
3.27
Q2
4.31
Q4
86.1
Q3
6.37
c
Q1
5.65
Q2
4.01
Q4
82.6
Q3
7.72
d
Q1
0.037
Q2
0.050
Q4
92.9
Q3
7.03
e
Q1
1.47
Q2
14.9
Q4
77.5
Q3
6.09
FL3-H
FL1-H

Figure 2

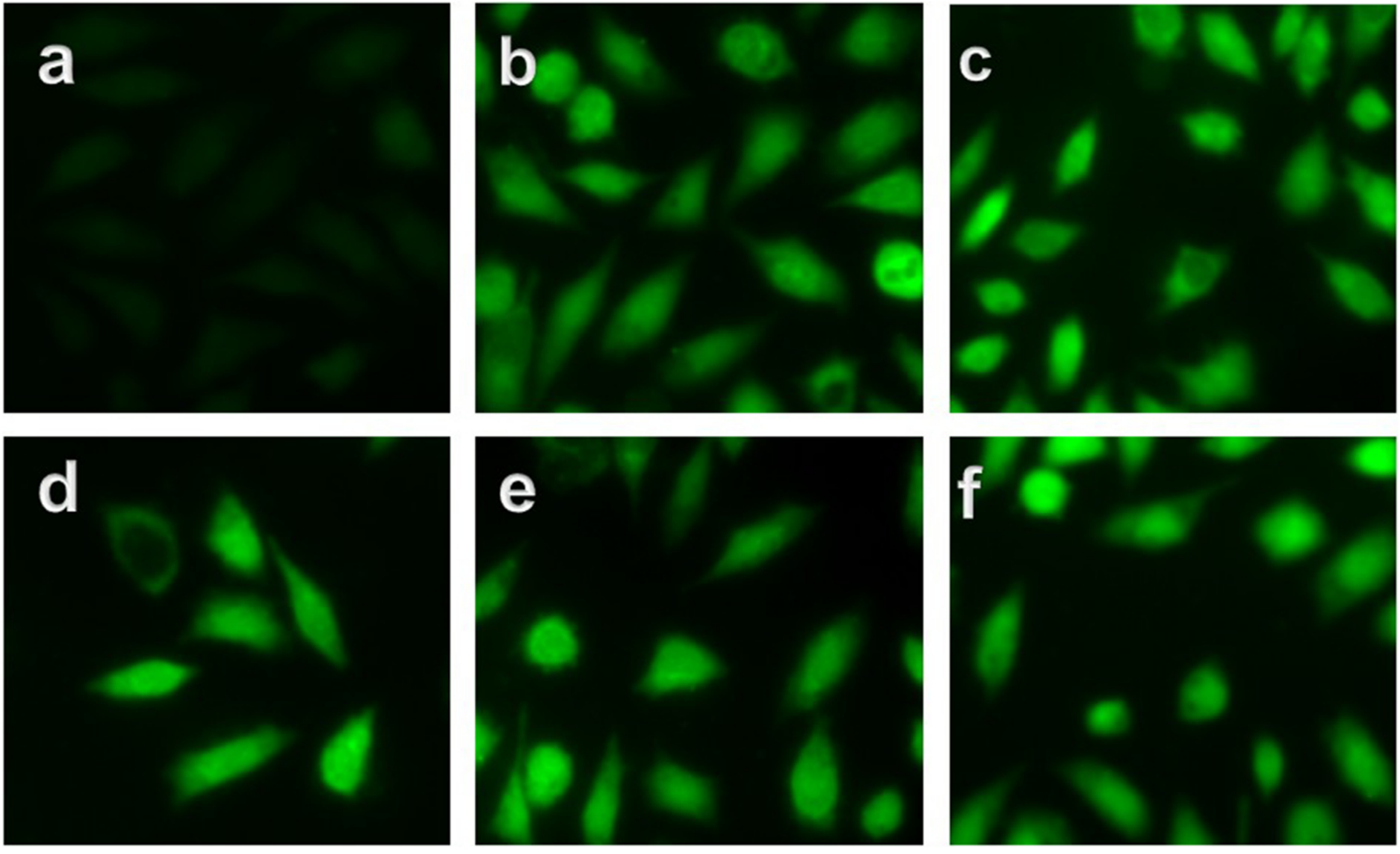

Figure 3

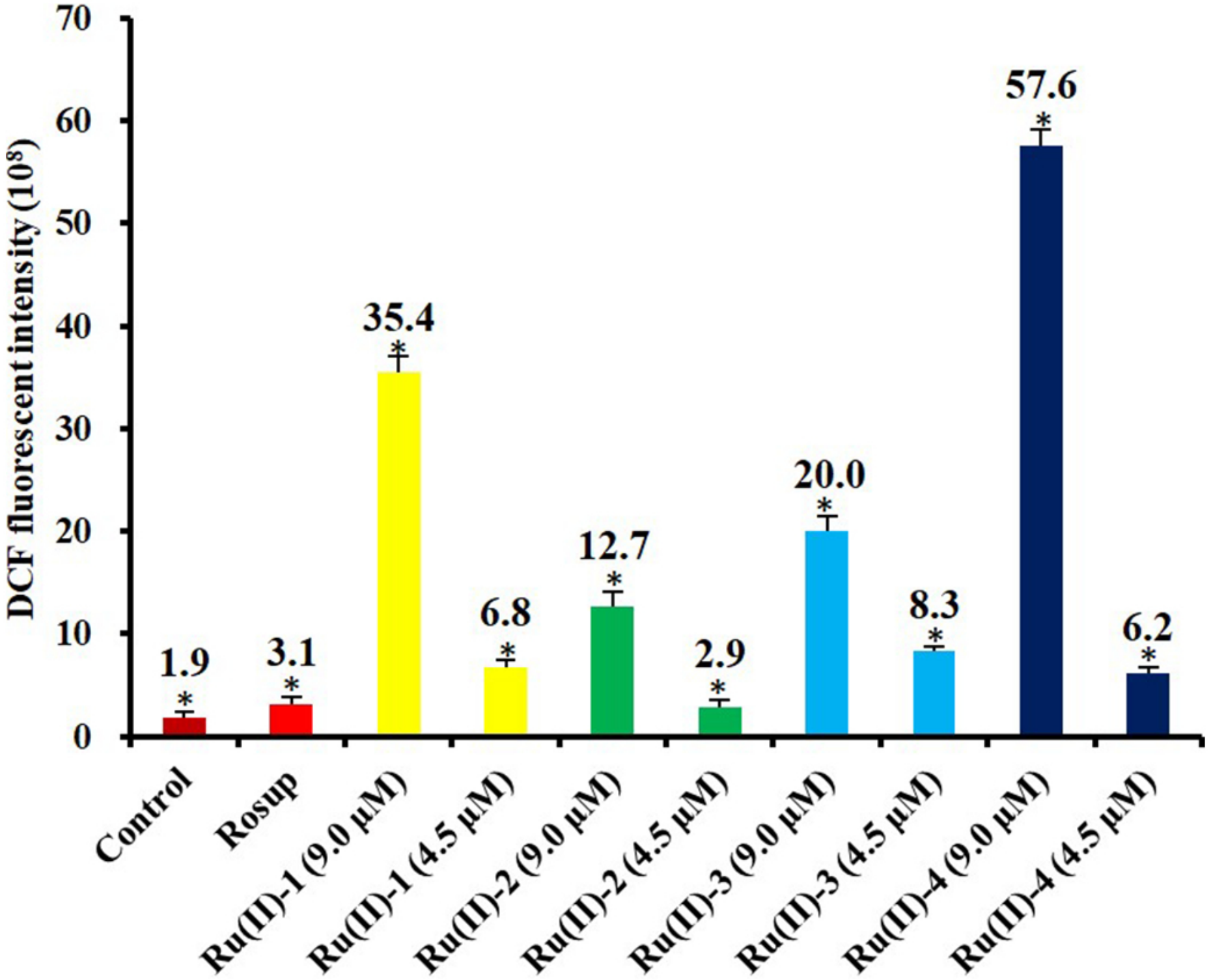
DCF fluorescent intensity (10^8)
70
60
50
40
30
20
10
0
1.9
3.1
35.4
6.8
12.7
2.9
20.0
8.3
57.6
6.2
*
Control
Rosup
Ru(II)-1 (9.0 μM)
Ru(II)-1 (4.5 μM)
Ru(II)-2 (9.0 μM)
Ru(II)-2 (4.5 μM)
Ru(II)-3 (9.0 μM)
Ru(II)-3 (4.5 μM)
Ru(II)-4 (9.0 μM)
Ru(II)-4 (4.5 μM)

Figure 4

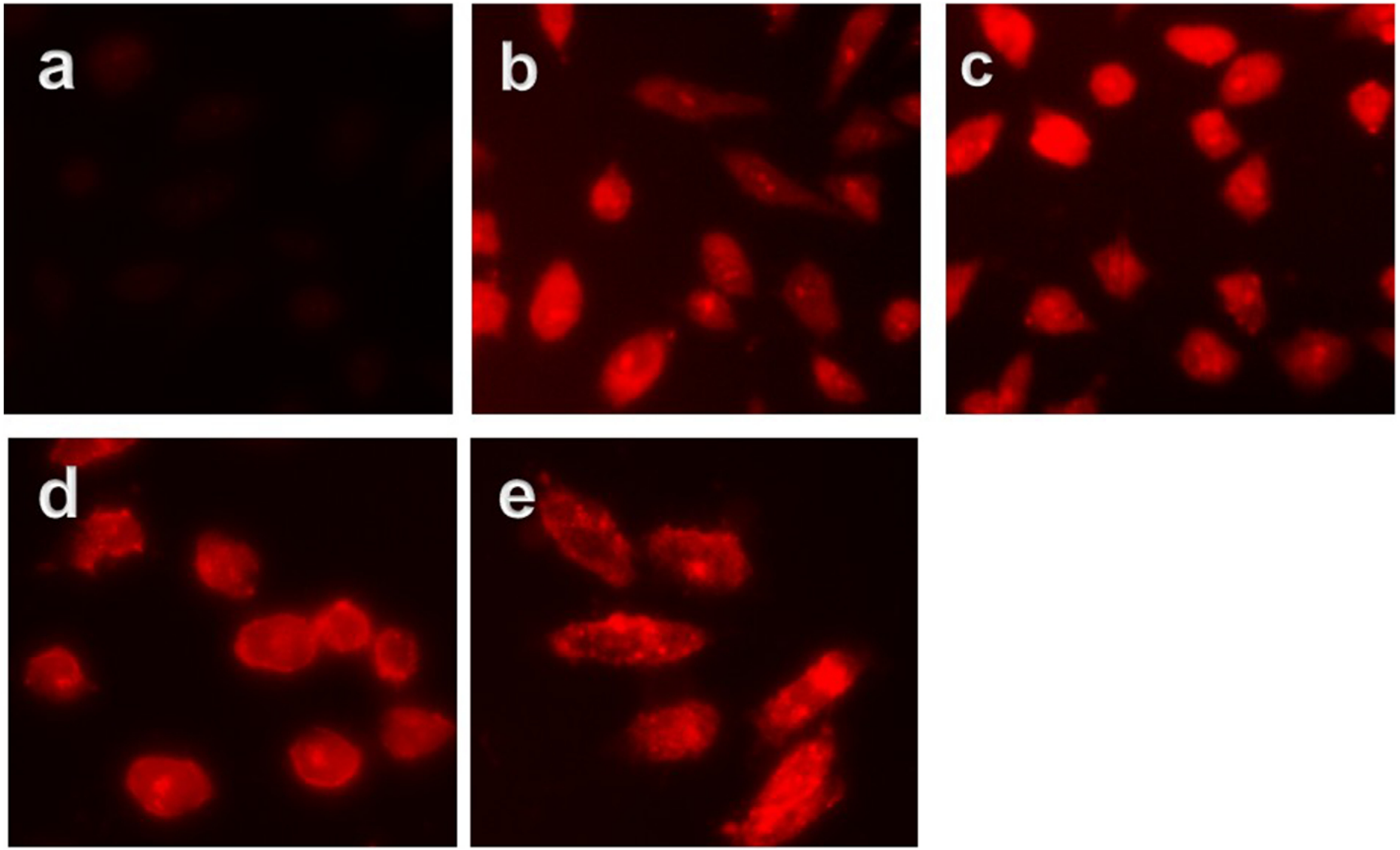

Figure 5

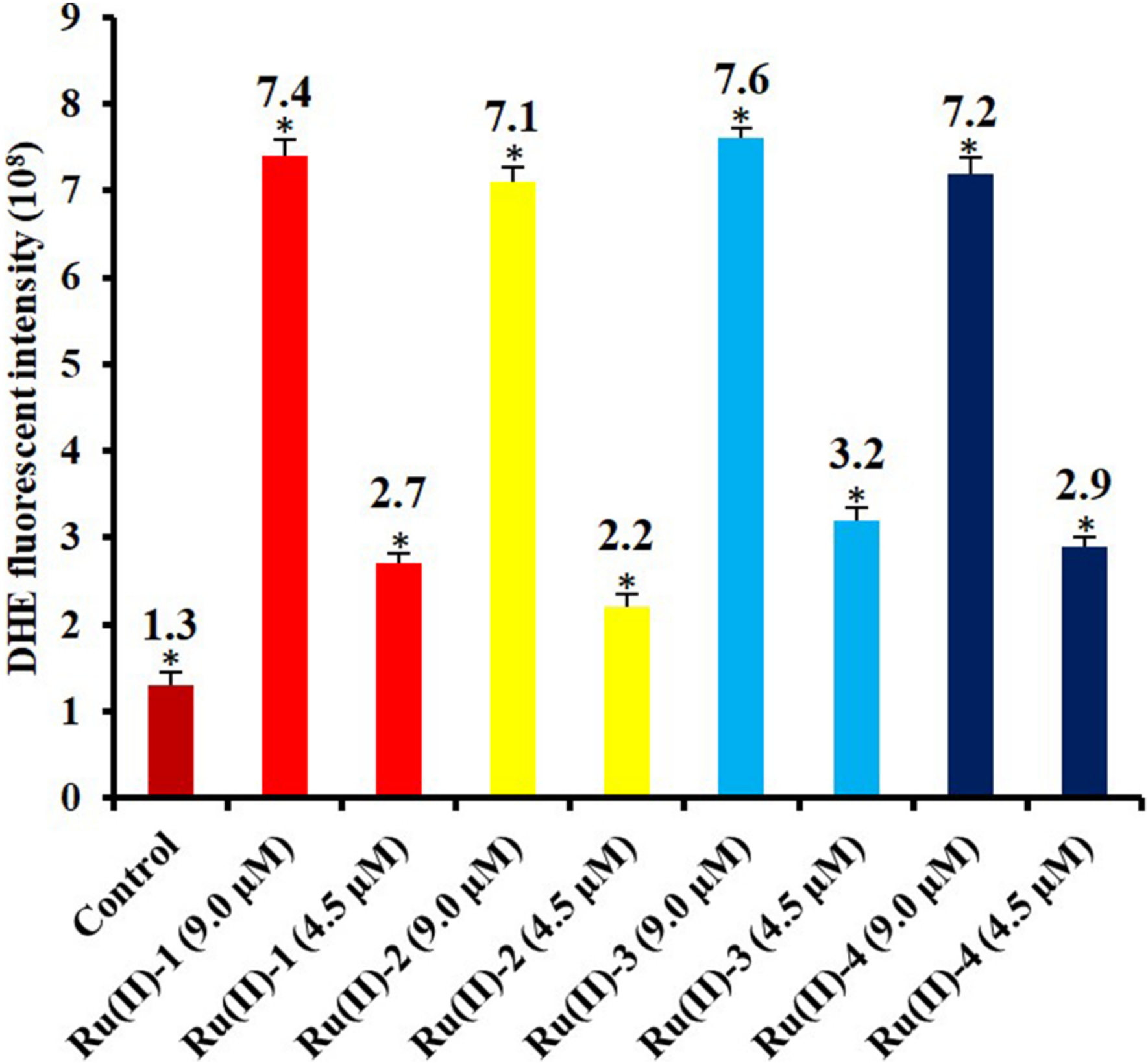
DHE fluorescent intensity (10⁸)
0
1
2
3
4
5
6
7
8
9
1.3
*
7.4
*
2.7
*
7.1
*
2.2
*
7.6
*
3.2
*
7.2
*
2.9
*
Control
Ru(II)-1 (9.0 μM)
Ru(II)-1 (4.5 μM)
Ru(II)-2 (9.0 μM)
Ru(II)-2 (4.5 μM)
Ru(II)-3 (9.0 μM)
Ru(II)-3 (4.5 μM)
Ru(II)-4 (9.0 μM)
Ru(II)-4 (4.5 μM)

Figure 6

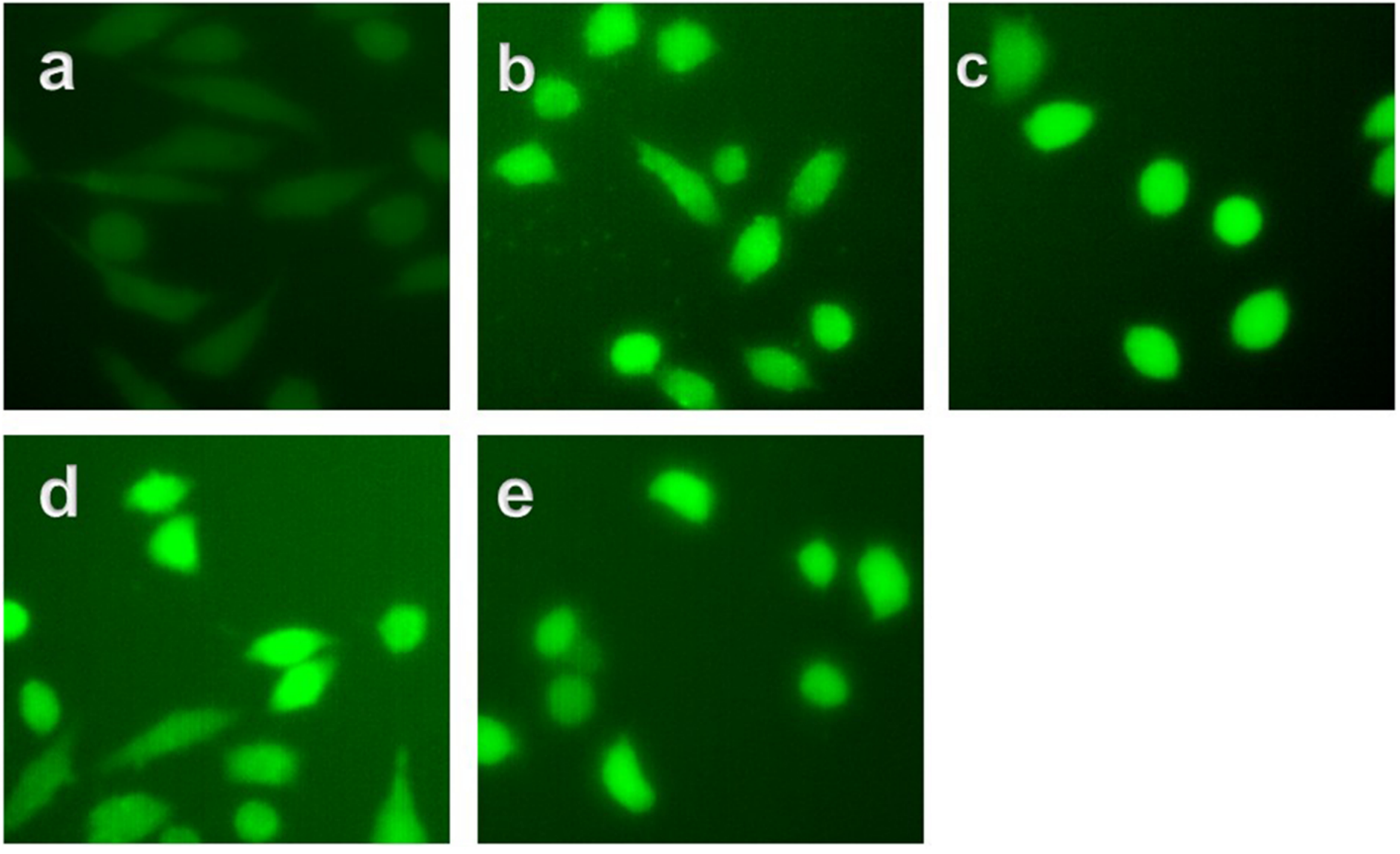

Figure 7

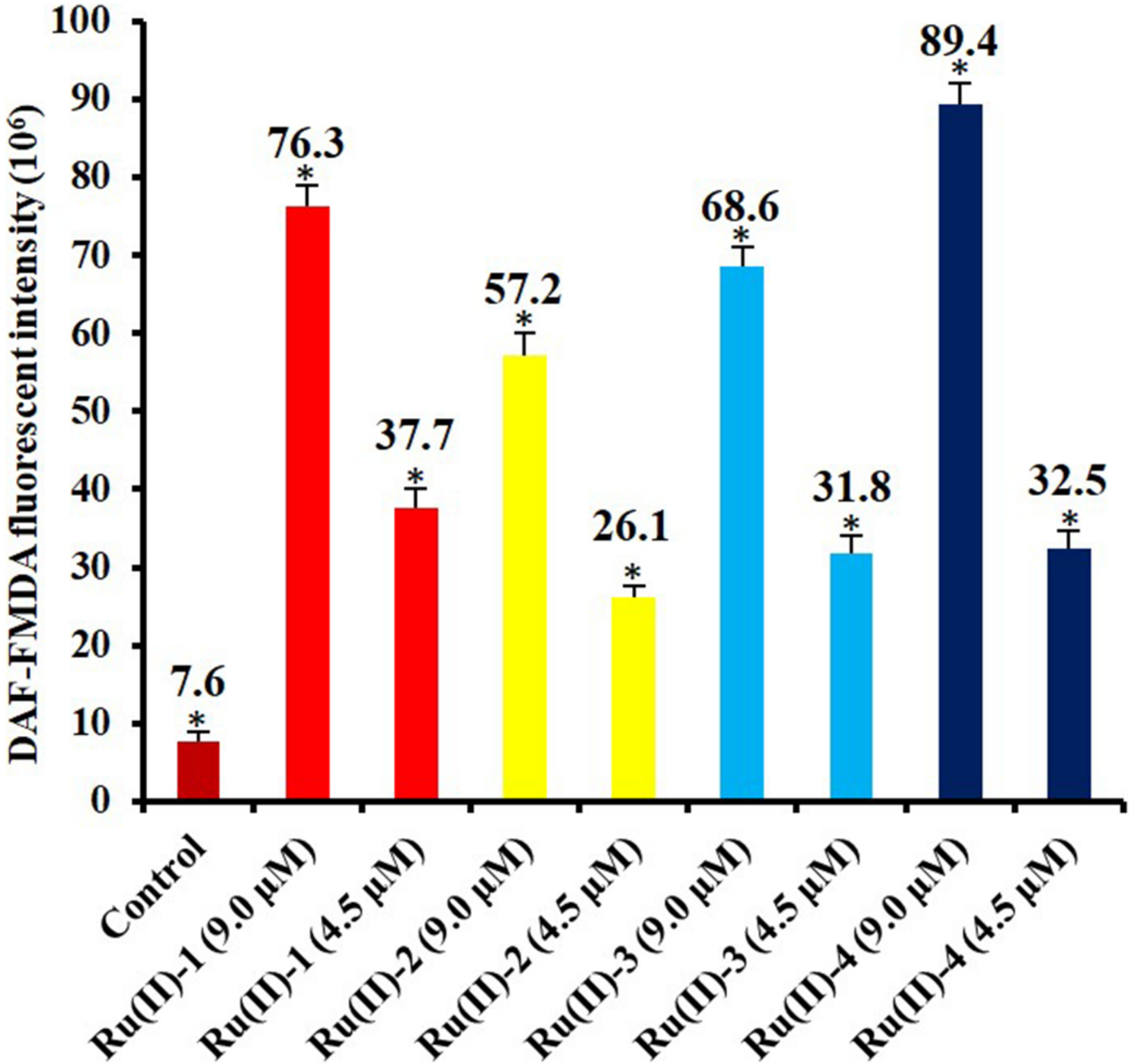
DAF-FMDA fluorescent intensity (10⁶)
100
90
80
70
60
50
40
30
20
10
0
7.6
*
76.3
*
37.7
*
57.2
*
26.1
*
68.6
*
31.8
*
89.4
*
32.5
*
Control
Ru(II)-1 (9.0 μM)
Ru(II)-1 (4.5 μM)
Ru(II)-2 (9.0 μM)
Ru(II)-2 (4.5 μM)
Ru(II)-3 (9.0 μM)
Ru(II)-3 (4.5 μM)
Ru(II)-4 (9.0 μM)
Ru(II)-4 (4.5 μM)

Figure 8

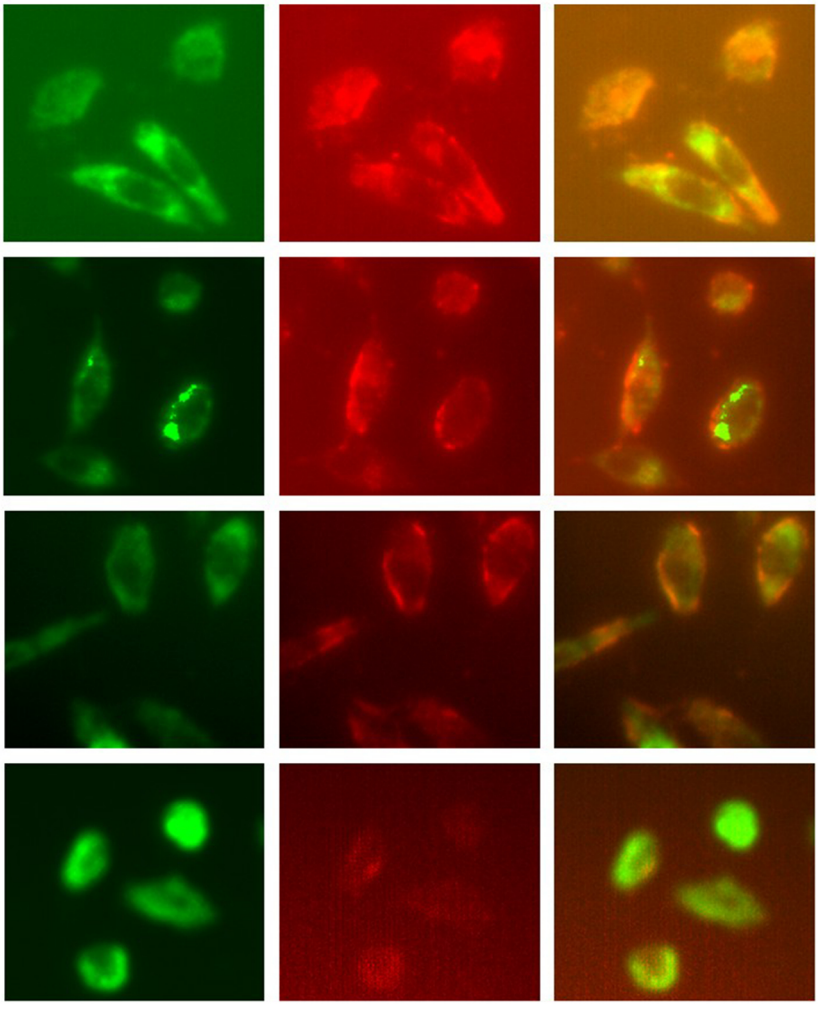
MitoTracker Green
Ru(II) (red)
Overlay
Ru(II)-1
Ru(II)-2
Ru(II)-3
Ru(II)-4

Figure 9

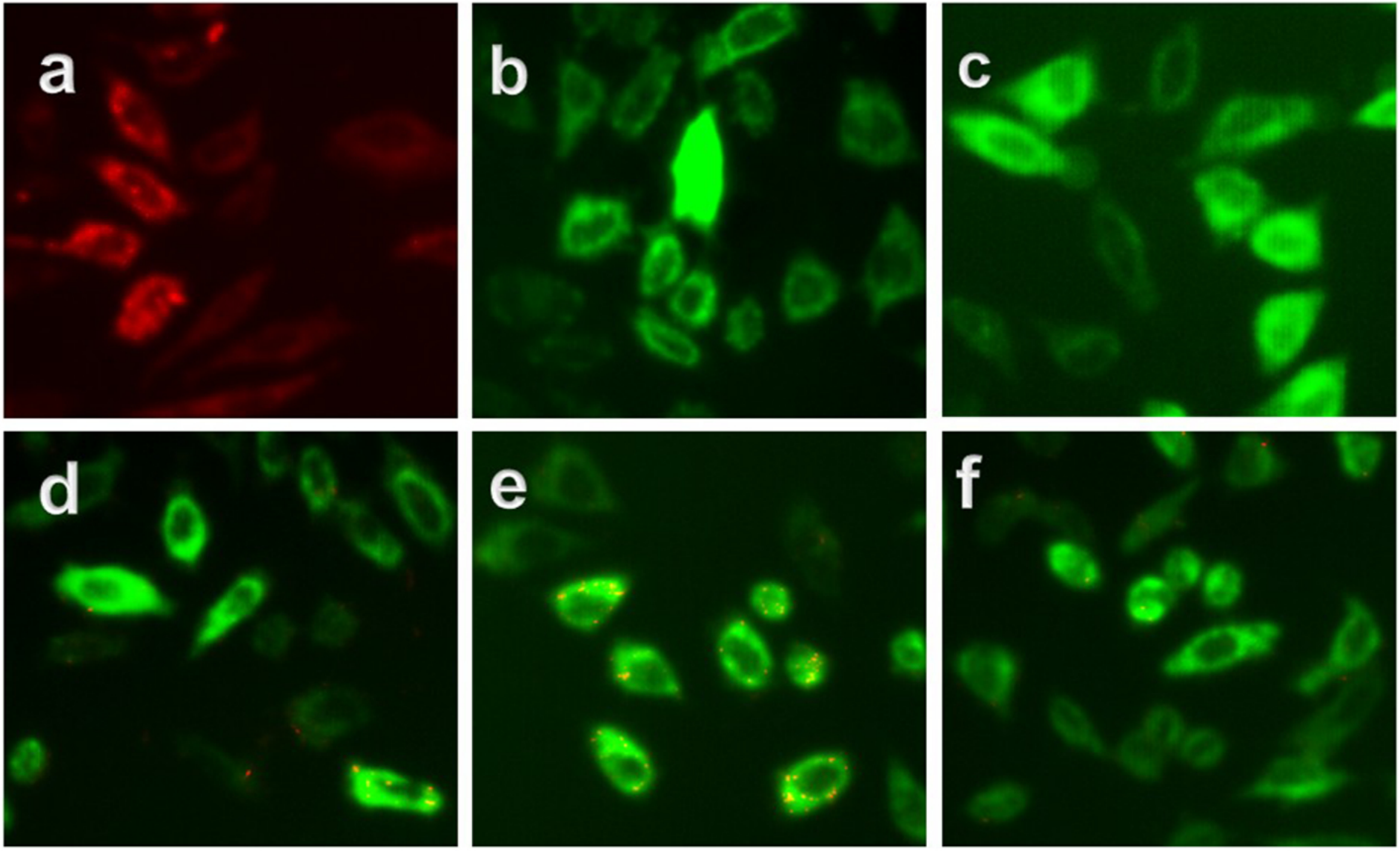

Figure 10

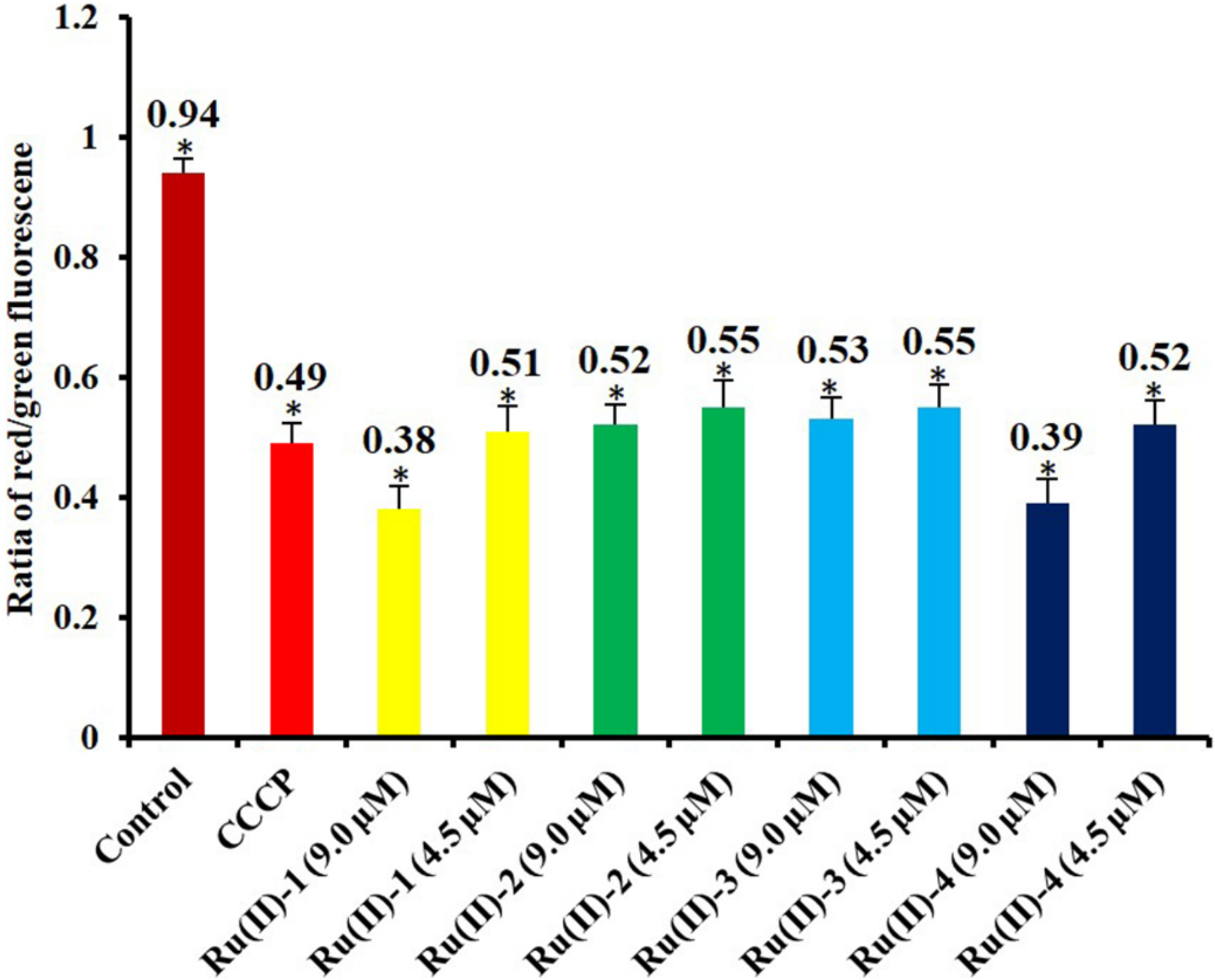
Ratia of red/green fluorescene
1.2
1
0.8
0.6
0.4
0.2
0
0.94
0.49
0.38
0.51
0.52
0.55
0.53
0.55
0.39
0.52
*
Control
CCCP
Ru(II)-1 (9.0 μM)
Ru(II)-1 (4.5 μM)
Ru(II)-2 (9.0 μM)
Ru(II)-2 (4.5 μM)
Ru(II)-3 (9.0 μM)
Ru(II)-3 (4.5 μM)
Ru(II)-4 (9.0 μM)
Ru(II)-4 (4.5 μM)

Figure 11

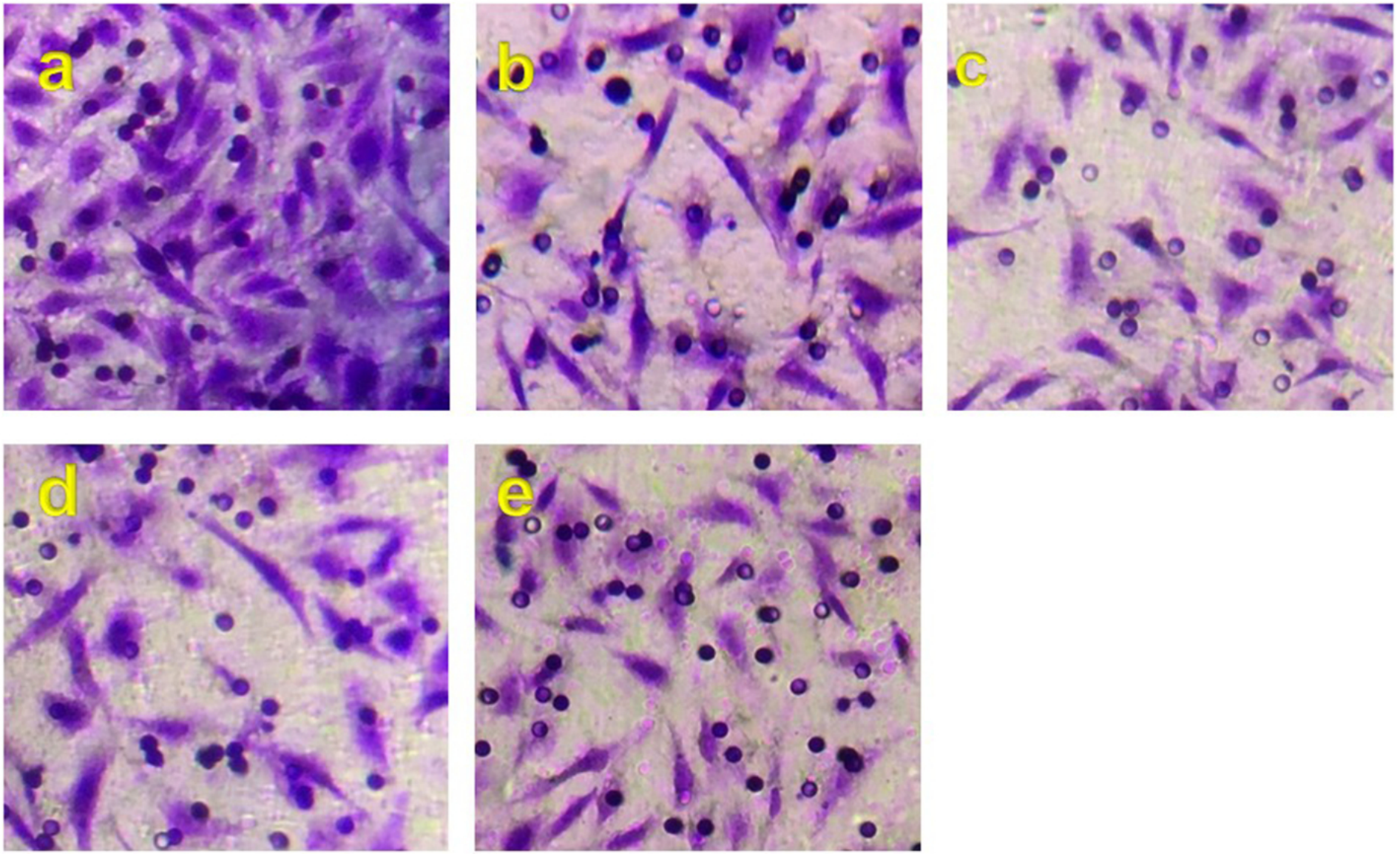

Figure 12

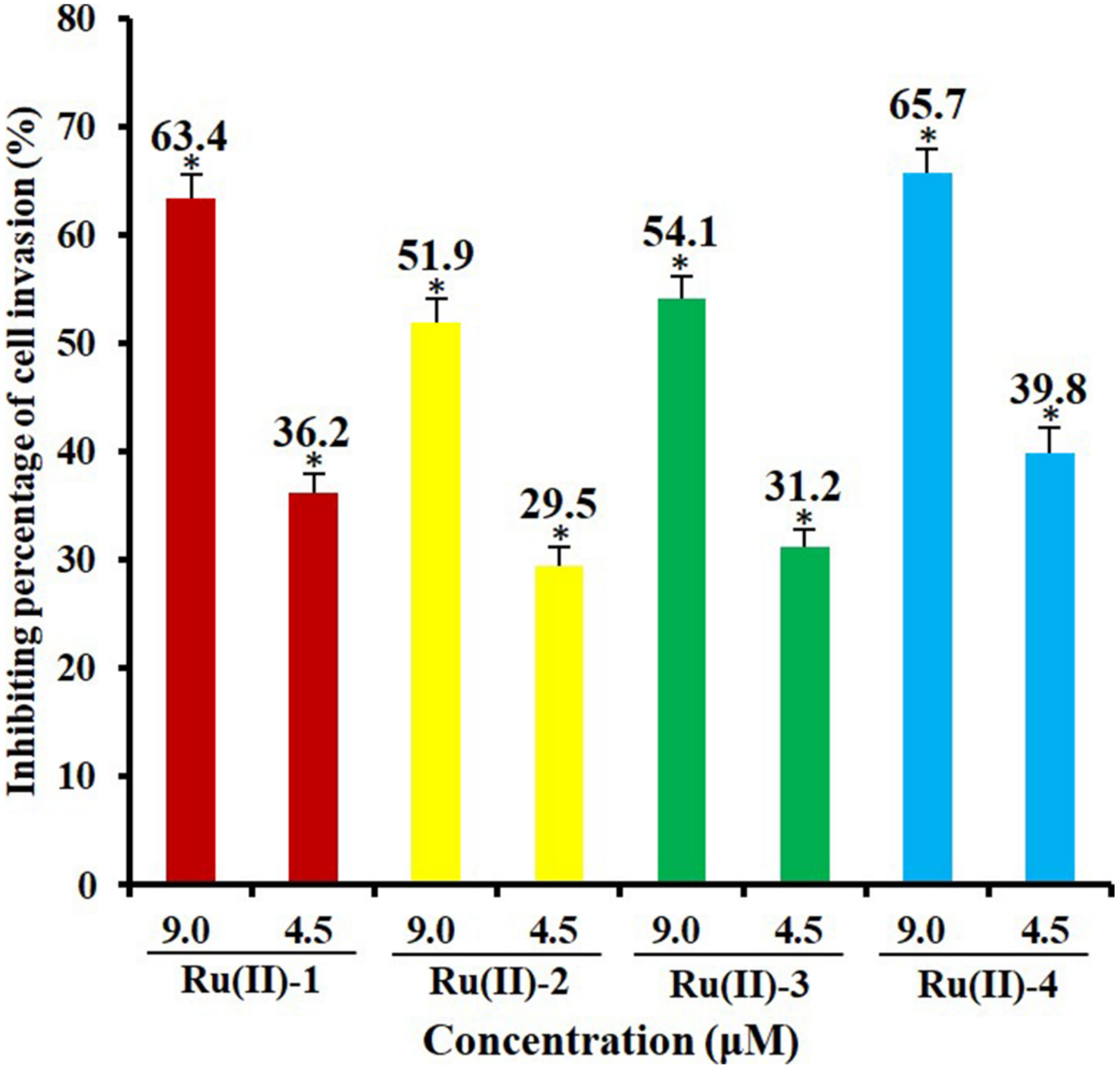
Inhibiting percentage of cell invasion (%)
80
70
60
50
40
30
20
10
0
63.4
*
36.2
*
51.9
*
29.5
*
54.1
*
31.2
*
65.7
*
39.8
*
9.0
4.5
9.0
4.5
9.0
4.5
9.0
4.5
Ru(II)-1
Ru(II)-2
Ru(II)-3
Ru(II)-4
Concentration (μM)

Figure 13

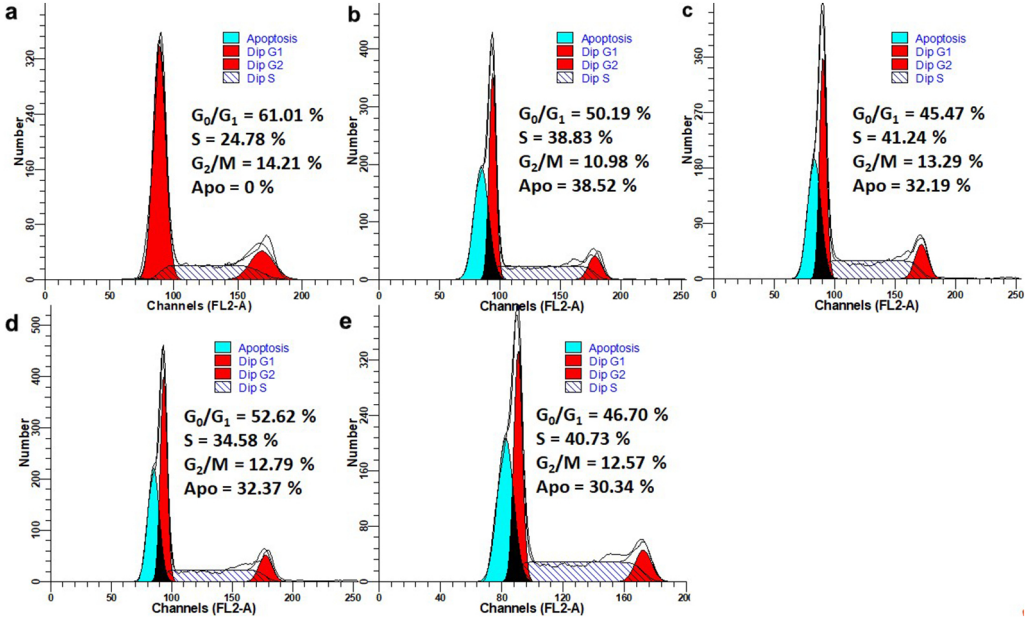
a
Apoptosis
Dip G1
Dip G2
Dip S
G0/G1 = 61.01 %
S = 24.78 %
G2/M = 14.21 %
Apo = 0 %
Number
Channels (FL2-A)
b
Apoptosis
Dip G1
Dip G2
Dip S
G0/G1 = 50.19 %
S = 38.83 %
G2/M = 10.98 %
Apo = 38.52 %
Number
Channels (FL2-A)
c
Apoptosis
Dip G1
Dip G2
Dip S
G0/G1 = 45.47 %
S = 41.24 %
G2/M = 13.29 %
Apo = 32.19 %
Number
Channels (FL2-A)
d
Apoptosis
Dip G1
Dip G2
Dip S
G0/G1 = 52.62 %
S = 34.58 %
G2/M = 12.79 %
Apo = 32.37 %
Number
Channels (FL2-A)
e
Apoptosis
Dip G1
Dip G2
Dip S
G0/G1 = 46.70 %
S = 40.73 %
G2/M = 12.57 %
Apo = 30.34 %
Number
Channels (FL2-A)

Figure 14

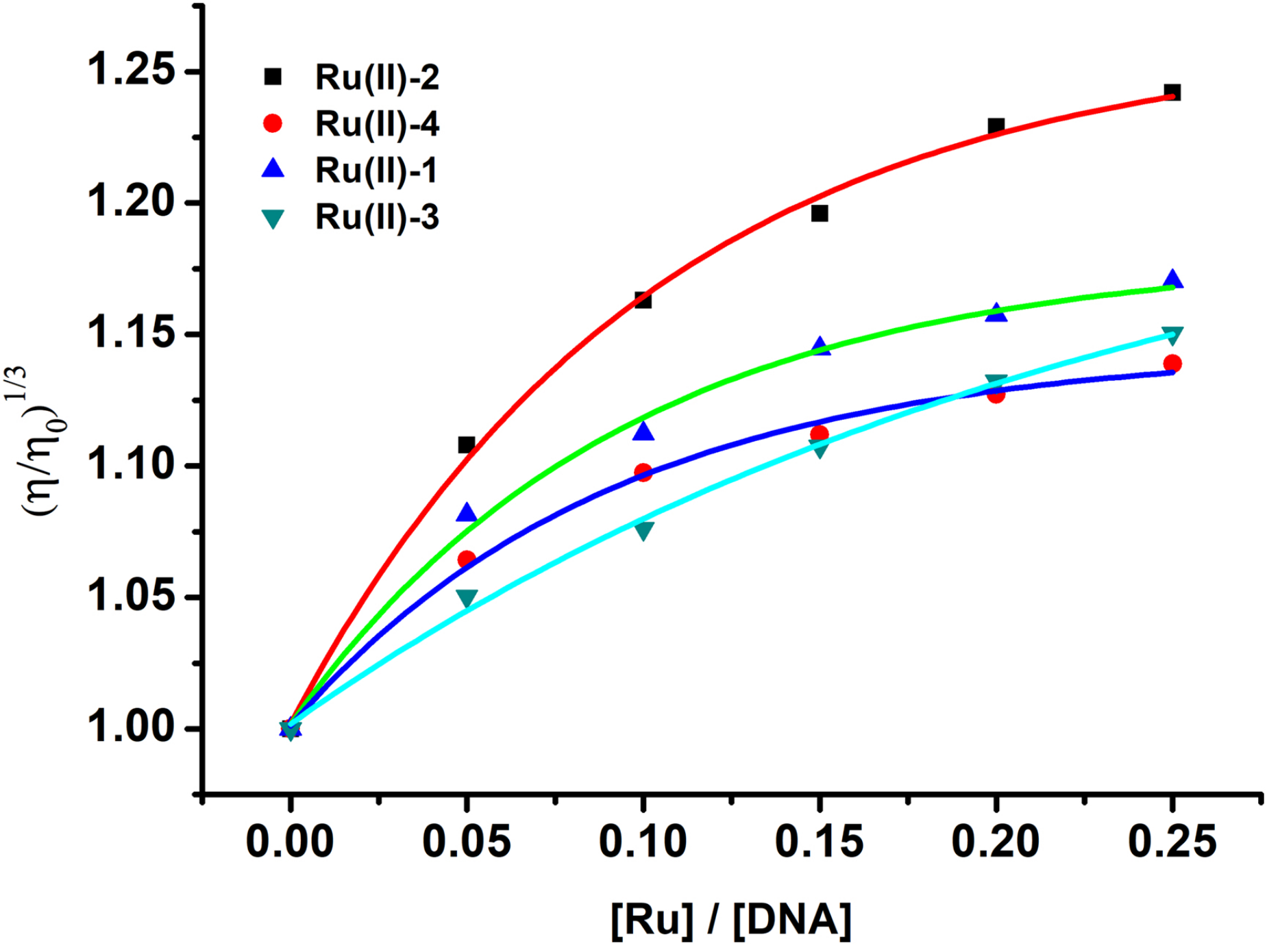
Ru(II)-2
Ru(II)-4
Ru(II)-1
Ru(II)-3
1.25
1.20
1.15
1.10
1.05
1.00
$(\eta/\eta_0)^{1/3}$
0.00
0.05
0.10
0.15
0.20
0.25
[Ru] / [DNA]

Figure 15

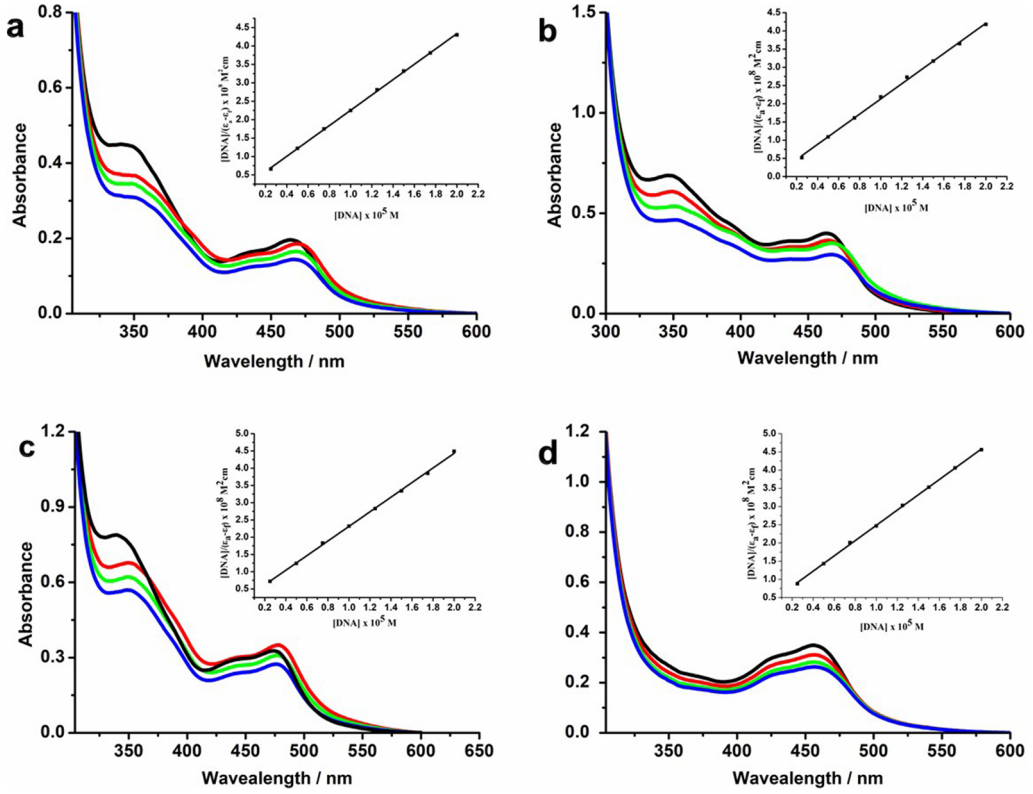
a
Absorbance
Wavelength / nm
[DNA]/(εa-εf) x 10^5 M^2cm
[DNA] x 10^5 M
b
Absorbance
Wavelength / nm
[DNA]/(εa-εf) x 10^8 M^2cm
[DNA] x 10^5 M
c
Absorbance
Wavealength / nm
[DNA]/(εa-εf) x 10^8 M^2cm
[DNA] x 10^5 M
d
Absorbance
Wavealength / nm
[DNA]/(εa-εf) x 10^8 M^2cm
[DNA] x 10^5 M

Figure 16

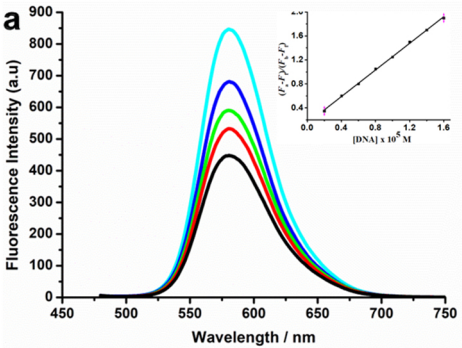
a
Fluorescence Intensity (a.u)
Wavelength / nm
[DNA] x 10^5 M

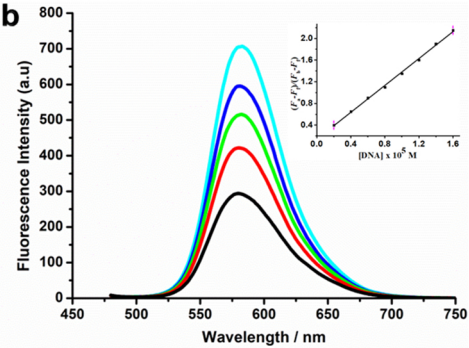
b
Fluorescence Intensity (a.u)
Wavelength / nm
[DNA] x 10^5 M

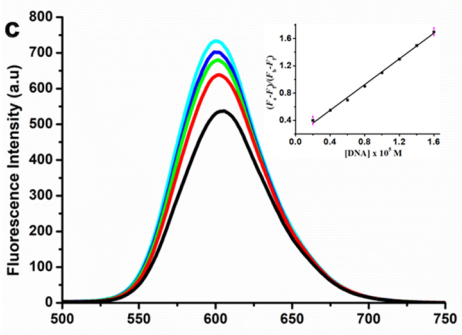
c
Fluorescence Intensity (a.u)
Wavelength / nm
[DNA] x 10^5 M

Figure 17